Cotton mercerization studied by a combination of microdrop generator and synchrotron radiation microdiffraction

Masterthesis

Dem Prüfungsausschuss für Chemie/Molecular Science
der Naturwissenschaftlichen Fakultät II
der Friedrich-Alexander-Universität Erlangen-Nürnberg

vorgelegt von

Johannes M. Schöck

aus Fürth

2007

Index

1 INTRODUCTION 2

2 CELLULOSE 3

2.1 Chemical structure 3
2.2 Crystallographic structures 4
2.3 Fibrillar morphology 4
2.4 Industrial cellulose transformation (Mercerization) 5
2.5 Chemical and structural processes during mercerization 7

3 X-RAY SCATTERING 9

3.1 Introduction 9
3.2 Structural analysis of polymeric materials 10
3.3 Simulation of a cellulose fiber diffraction pattern 13
3.4 Introduction into microdiffraction 14
3.5 The ID13 microdiffraction beamline 14

4 EXPERIMENTAL METHODS 16

4.1 Materials 16
4.2 Instrumentation & sample environment 17
4.2.1 X-ray set-up 17
4.2.2 Stretching cell 19
4.2.3 Microdrop generator 20
4.3 Data calibration and analysis 21
4.3.1 Data calibration 21
4.3.2 Analysis of individual patterns and sequences of patterns 22

5 RESULTS & DISCUSSION 23

5.1 Basic structures 24
5.2 Cotton hydration 25
5.3 Formation of sodium-cellulose 27
5.4 Formation of other alkali-cellulose phases 37

6 CONCLUSION AND OUTLOOK 39

ANNEX A: PREPARATION OF SOLUTIONS AND FIBERS 41

ANNEX B: PRACTICAL ASPECTS OF MICRODROP GENERATOR 42

ANNEX C: FILES AND DATES 43

LITERATURE 44

ACKNOWLEDGEMENTS 48

1 Introduction

The aqueous NaOH induced transformation of cellulose I into cellulose II proceeds through at least one and probably more intermediate Na-cellulose crystalline phases [1, 2]. Structural studies suggest that the conversion from the parallel-chain structure of cellulose I into the antiparallel-chain structure of cellulose II occurs already in this step [3].

The aim of the current master thesis was to develop an experimental setup which allows studying this step - also for similar systems - in more detail using synchrotron microbeam diffraction techniques developed at the ESRF ID13 beamline [4]. Of particular interest was to obtain local structural information on single cellulose fibers as compared to X-ray experiments on fiber bundles, which online give averaged structural information. A further aim was to use a microdrop generator [5-7] in order to locally initiate the structural transformations in a well defined reaction volume.

Today polymeric fibers are of great importance in the industry and every day use. A setup to study single fibers and their chemical reactions in an exact manner can help to develop new applications for existing products and to find new materials with sought for properties.

Since the master project is limited to six months, only a part of the experiments performed is presented here. Selected diffraction patterns and sequences of diffraction patterns (scans) have been analyzed and are presented below in order to show the power of the techniques in monitoring local structural changes. It is hoped that this will put a new impetus on structural studies during mercerization and other structural transformations using the newly developed setup and techniques.

2 Cellulose

2.1 Chemical structure

Cellulose is the most abundant biopolymer on earth, occurring largely in plants, but also in bacteria and algae. Plants use cellulose to construct cell walls, which need to be rigid and flexible at the same time, to compensate for pressure on the plant.

The chemical structure of cellulose shown in Fig.1 corresponds to a linear syndiotactic polymer of D-anhydroglucopyranose units (AGU) linked by β-(1,4)-glycosidic bonds. One can also regard cellulose as the isotactic polymer of cellobiose, which is the dimer of AGU [8]. Cellulose from the cotton flower, which was used in this work, has a degree of polymerization (DP) of as much as n≈4200 for untreated and a considerably lower DP of n<2000 for extensively processed cotton [9, 10]. The generally assumed conformation of the AGU in the cellulose chain is a $^4C_1$ chair with the hydroxyl groups in equatorial and the hydrogen atoms in axial positions [11].

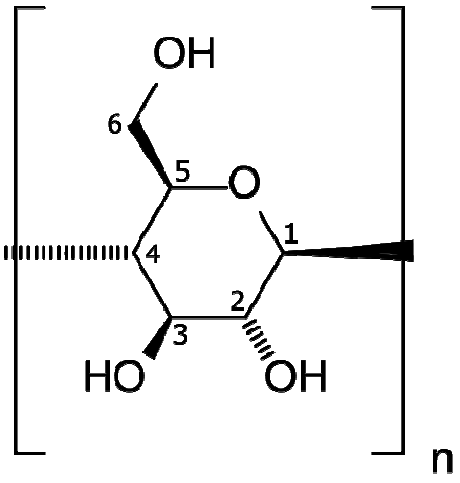

Fig.1 Repetitive unit of cellulose: poly(1,4'-O-β-D-glucopyranoside)

2.2 Crystallographic structures

Cotton in its natural form consists almost exclusively of a fraction of crystalline cellulose I domains embedded in an amorphous matrix. High-resolution ^{13}C cross polarization magic angle spinning (CP/MAS) NMR [12, 13], as well as electron, X-ray and neutron fiber diffraction [14, 15] have shown that cellulose I can adopt two allomorphic structures, which were named cellulose I_α (triclinic) and cellulose I_β (monoclinic). Natural synthesis produces both kinds in various proportions, depending on the biological origin; I_α being found more in algae and bacteria while I_β is the major form in higher plants and animals. For the cellulose I_α and I_β structures, the conformation of the hydroxymethyl group (C-6) is trans-gauche (t-g) [16].

Cellulose I can be transformed into several other modifications. The important one in the context of this work is cellulose II, which is formed during mercerization (section 2.4 and 2.5), while cellulose III (from ammonia treatment of cellulose I [17]) and IV (from glycerol treatment of cellulose II [18]) is not known to play a role during mercerization [19-21].

Cellulose gets its stability from a number of intra- and intermolecular hydrogen bonds between the oxygen atoms and the hydroxyl groups. Detailed hydrogen-bonding models and complete crystal structures including hydrogen atom positions have been proposed based on X-ray and neutron diffraction data of cellulose I_α & I_β [14, 15, 19].

2.3 Fibrillar morphology

A single cellulose fiber is composed of many microfibrils, which are made up from nanocrystalline domains, 10-35 nm wide and 3.5-10 nm thick, running in the same direction as the macroscopic fiber axis with a slight tilt angle of several degrees, depending on the cellulose source. The microfibrils are held together mainly due to the intermolecular hydrogen bonds and are embedded in an amorphous matrix. The matrix consists of faulty cellulose chains with partially broken hydrogen bonds and

irregular polymer helices [9, 22].[1] The super-helicoidal microfibril morphology [23] has recently been observed directly for single wood cells with synchrotron radiation [24].

The structural organization of the cellulose microfibrils is not yet completely unraveled, although most authors support the theory that cellulose I consists of parallel chains [13, 16, 25-27], while cellulose II features an antiparallel structure [28-32]. In order to explain the structural integrity of the fiber during the cellulose I to cellulose II transformation, the role of the amorphous parts between the nanocrystalline domains has been invoked [33]. In particular, it has been suggested that neighboring domains of cellulose I having opposite chain polarity could act as the nucleation site for the growth of antiparallel chain domains under the action of aqueous NaOH, which enters preferentially the amorphous zones [2, 34, 35]. An increase in void volume observed by SAXS during swelling of cellulose fibers in aqueous NaOH solution appears to support the assumption of a separation of elementary fibrils by the swelling agent [36]. This is corroborated by studies of mercerization at the microfibrillar level, which have shown that it is impossible for isolated cellulose microfibrils to become mercerized while keeping their initial microfibrillar morphology [37].

2.4 Industrial cellulose transformation (Mercerization)

Mercerization is a treatment for cotton fabric and thread mostly employed to give cotton a lustrous appearance and improved dye acceptance. The series of processes was devised by John Mercer in the middle of the 19th century. Mercerized cotton is sometimes referred to in the crafts as pearl or pearle cotton. Added desirable water handling properties gained are a secondary bonus.

In 1851, John Mercer was granted a British Patent for work he had done pertaining to cotton, linen and other vegetable fibrous materials that in effect caused certain changes in the character of the fiber when subjected to caustic soda, sulfuric acid, and/or other chemicals. He went on to list a number of these changes, one of

[1] review: www.lsbu.ac.uk/water/hycel.html

which was that caustic soda caused the fiber to swell, become round and straighten out (but it did not impart any change in luster). At the time Mercer introduced these processes, the British cotton trade showed no interest in any of it and it all sat in obscurity for about forty years. In 1890 Horace Lowe was granted a British patent in which he claimed that by applying Mercer's caustic soda process to cotton yarn or fabric under tension a resultant high luster (a result of the light reflection off the smooth, round surface) was imparted to the fiber. It became an overnight success and revolutionized the cotton industry [38].

Mercerization is also part of the industrial viscose production process. Viscose was first patented by Cross, Bevan & Beadle in Britain in 1892. The word viscose is believed to have been used by Cross to describe the product, although in the USA in the 1920s the word rayon was adopted. Viscose was first used for coating fabrics which it did quite successfully, while other ideas failed. Eventually, after Samuel Courtauld & Co. had taken over in 1904, viscose manufacture became big business. By the twenties and thirties it had almost completely replaced the traditional cotton and wool for women’s stockings and underwear. Similar changes occurred in the USA and in Europe, too. Viscose was also being used for linings and furnishing fabrics; providing the staple for towels and table-cloths and was being made into high tenacity yarn for tires. Yet other uses included the manufacture of sponges and absorbent cloths. Making viscose film had been tried by Cross in the 1890s but it was in Switzerland and France that major successes were achieved. By 1913 C.T.A. established La Cellophane SA. Ten years later DuPont Cellophane Co. was set up in the USA and in 1935 British Cellophane Ltd. was established.

Grenoble and the Isère region have a rich industrial history in viscose production. Thus viscose as the first artificial textile fiber was produced in 1884 by the Count Hilaire de Chardonnet at Vernay de Charette, in the north of Isère. Commercial viscose production in Grenoble started in 1927 and went on until 1989, when Cellatex closed its Grenoble plant. Nowadays the "Musée de la Viscose" provides a rich collection of this important period of industrial development in Grenoble.

2.5 Chemical and structural processes during mercerization

Mercerization can be achieved by applying aqueous NaOH, or other alkaline-hydroxyl bases, to cellulose, provided that the fibers were cleaned from wax or the lignin removed from the wood chips [10]. The minimal base concentration required for successful mercerization has been reported to be 9% (= 2.25N) NaOH for primary wall cellulose [37] and between 10 and 14% (= 2.5 – 3.5N) for secondary wall cellulose [10].

The chemical reaction mechanism of mercerization is not yet known, although it is strongly suggested that the Na^+-ions of NaOH interact with the hydroxyl groups of the AGU (D-anhydroglucopyranose units) to form Na-cellulose, effectively swelling the fibers in the process. Other alkaline ions show the same behavior with moderately different diffraction patterns (see section 5.4), due to different ion radii. After reaching the intermediate alkali-cellulose step reconversion to cellulose I [39] as well as transformation to cellulose II, and several less important cellulose types [19, 20], are possible, depending on the procedure.

Structural changes during the transformation of cellulose I to cellulose II were reported to involve a change of chain polarity from parallel to anti-parallel [13, 16, 25-32]. Given that this would require either a flip of entire polymer chains or a reconstruction of the chains on a molecular level further investigations were conducted and an interdigitation mechanism was suggested. Here neighboring domains of parallel, but differently directed, microfibrils mingle during the reaction and new domains of antiparallel microfibrils are created [2, 34, 35]. Interdigitation was reported to already take place during the formation of Na-cellulose [3]. With this mechanism the problems of reversibility and inverting of chains no longer have to be considered, since the microfibrils only reorganize their position relative to each other and can stay intact in the process.

A number of different varieties of sodium- and other alkali-celluloses have been proposed, which were created through different base concentrations and reaction conditions and differ by the amount of NaOH and H_2O which is included into

the crystal lattice, hence also by the lattice parameters [10]. In Fig. 2 the proposed relations between the different structures are shown.

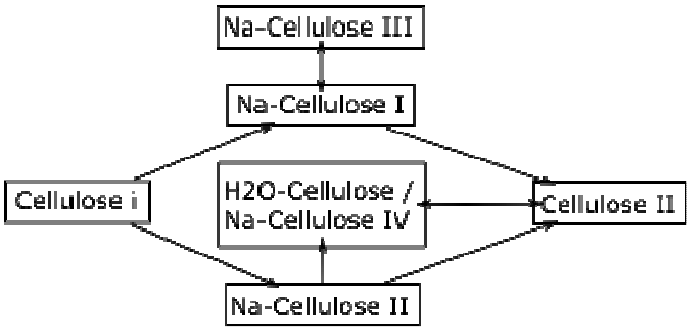

Fig.2 Possible paths of cellulose conversions with different H_2O and NaOH concentrations [2, 10].

Na-cellulose I, which formed during the experiments reported below, forms quickly in aqueous NaOH of a concentration of 10 – 20 mass-% (= 2.5 – 5N) [2]. From 19 – 45% NaOH, Na-cellulose II forms, resulting in mixtures of Na-cellulose I and II at the lower concentration level. Na-cellulose III is reversibly obtained from Na-cellulose I if the latter is dried or no H_2O is present, as is the case for NaOH dissolved in ethanol. If Na-cellulose I is washed thoroughly, cellulose II results. Washing Na-cellulose II with H_2O leads to water-cellulose, which was called originally Na-cellulose IV by its discoverers, while low NaOH concentrations convert it directly into cellulose II.

3 X-ray scattering

3.1 Introduction

The interaction of X-rays with matter is described in a number of textbooks [40-42]. Fig.3 shows schematically selected interactions, which are of particular interest in the context of the present work. The main interest for diffraction experiments on organic and polymeric materials is in maximizing elastic scattering and minimizing radiation damage.

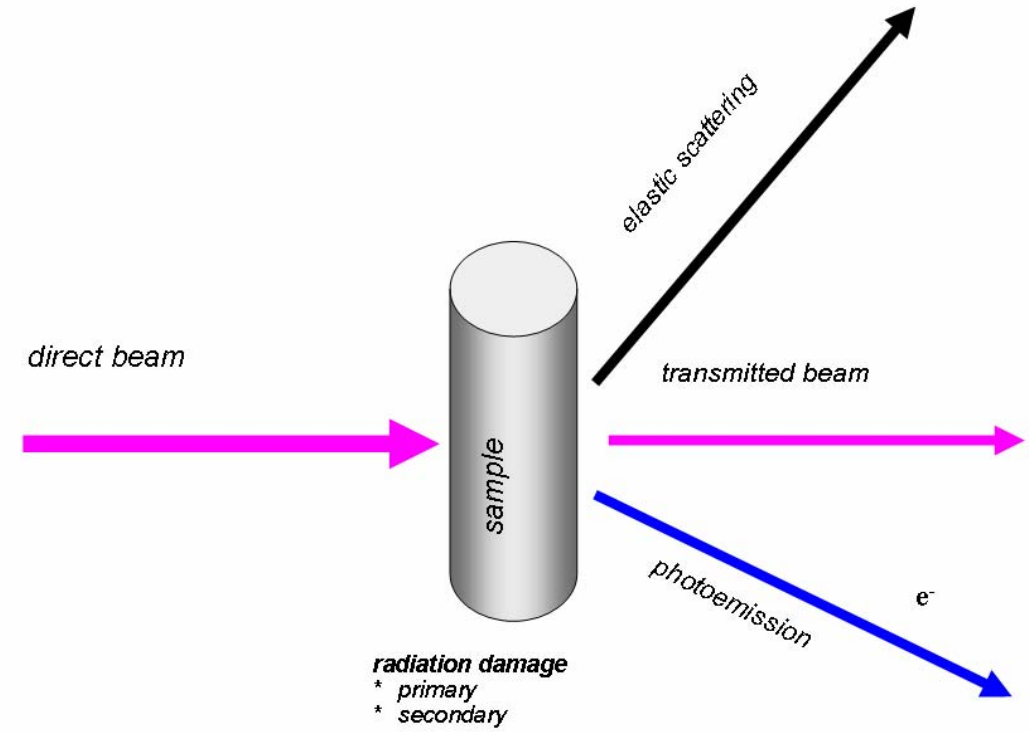

Fig.3 Schematic design of selected interactions of X-rays with matter.

The major part of the direct beam is not absorbed but is transmitted through the sample without change in energy. A fraction of the direct beam is elastically scattered, without change of energy. Another fraction of the direct beam interacts inelastically with matter, resulting in the formation of photoelectrons, which is the cause of primary and secondary radiation damage. This is particularly true for organic and biological crystals, where photoemission can create radicals, which can disrupt bonds [43, 44]. The elastic scattering process is shown as a vector diagram in Fig.4.

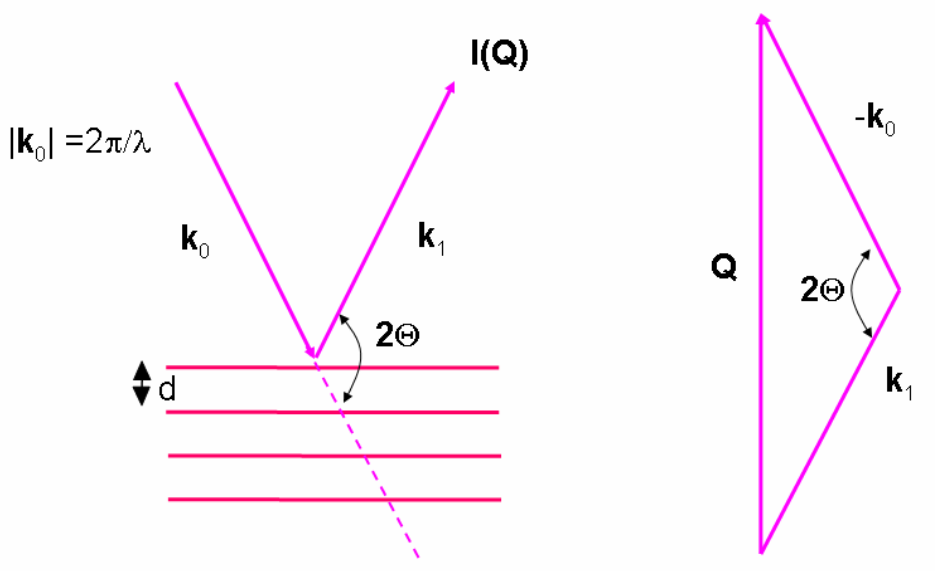

Fig.4 Schematic vector design of elastic scattering and Bragg equation.

Here $\mathbf{k_0}$ is the incoming radiation vector and $\mathbf{k_1}$ the outgoing radiation vector (vectors written in "bold"). For elastic scattering one can write: $|\mathbf{k_0}|=|\mathbf{k_1}|$. The so-called scattering vector **Q** can be written as: $\mathbf{Q}= \mathbf{k_1}- \mathbf{k_0}$ with its modulus $Q=(4\pi\sin\Theta)/\lambda$. Elastic scattering is usually called "diffraction" for a crystalline lattice, resulting in discrete reflections. In this case Bragg's equation applies:

$$n\lambda=2d\sin\Theta \qquad (1)$$

where Θ: Bragg angle; λ: wavelength; d: lattice spacing; n: diffraction order.

3.2 Structural analysis of polymeric materials

Synthetic and biological polymer fibers are known to be hierarchically organized materials [45] with order extending from the macroscopic to the atomic scales as shown schematically for a flax fiber in Fig.5 (see also sections 2.2 and 2.3).

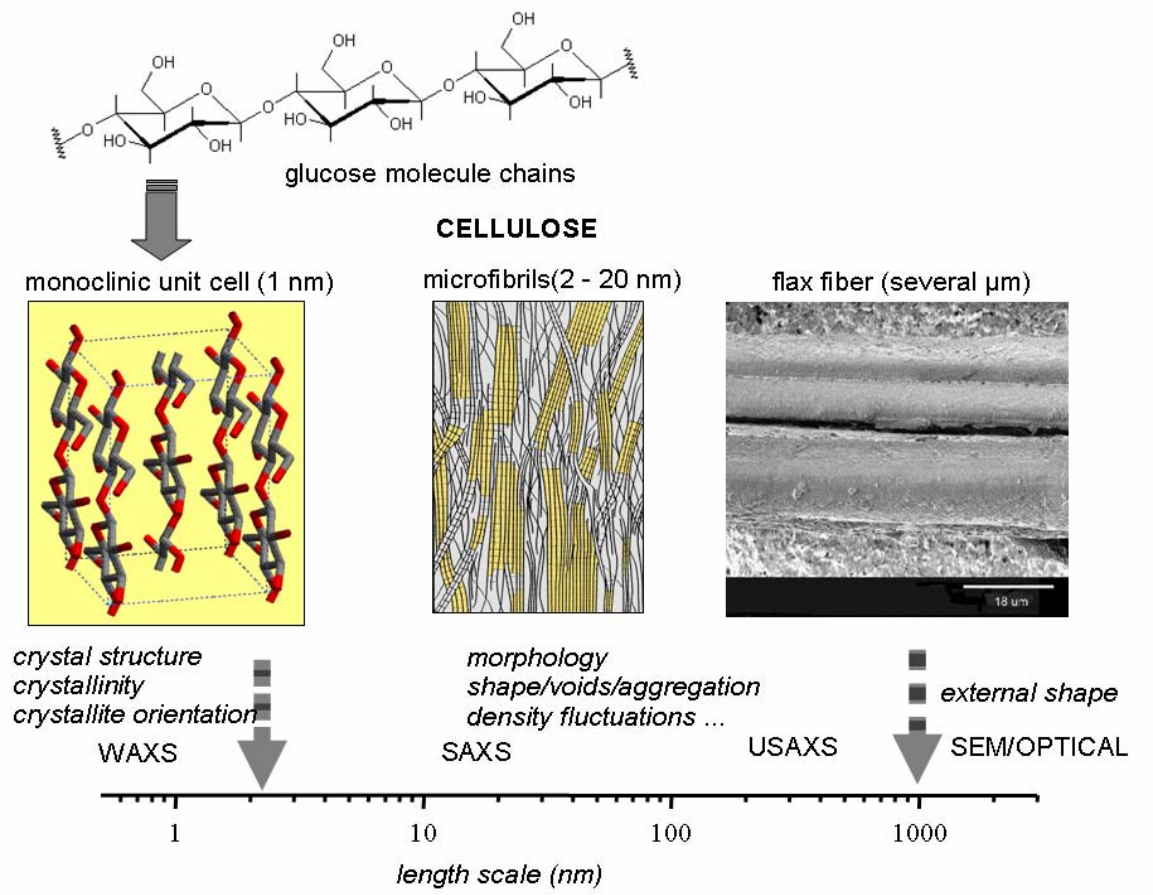

Fig.5 Schematic design of the hierarchical fiber organization of a cellulose fiber. The flax fiber image has been obtained by scanning electron microscopy (SEM): www.swicofil.com/products/003 flax.html. The length scales covered by different X-ray scattering and imaging techniques are also shown. The exact position of the overlap of techniques on the length scale is arbitrary.

Electron scattering techniques, which are used extensively for polymeric fiber analysis [46], require extensive sample preparation like sectioning and have very limited in-situ capabilities. X-ray scattering techniques are, however, ideal tools for in-situ studies, but provide in general only average information on an ensemble of fibers. As will be shown below, X-ray microdiffraction techniques using synchrotron radiation nowadays provide also local information, while retaining their excellent in-situ capabilities.

The different X-ray scattering techniques like wide-angle X-ray scattering (WAXS), small-angle X-ray scattering (SAXS) and ultra small-angle scattering (USAXS) [41] cover the hierarchical length scales shown in Fig.5. Thus WAXS techniques address the level of the unit cell, while SAXS/USAXS techniques address “morphological” scales and extend up to the optical scale.

The composite morphology of microfibrils embedded in an amorphous medium is also observed for many semicrystalline polymers. The X-ray diffraction pattern of

such materials consists of broad Bragg peaks due to the presence of nanometer-sized crystalline domains superimposed on a diffuse background due to the randomly oriented chains. The crystalline domains are composed of a finite number of unit cells, which constitute the smallest volume elements needed to fully describe the crystal [47]. The 3D arrangement of polymer chains in a crystalline domain is therefore completely described by a single unit cell. In general, one of the unit-cell axes (usually the **c** axis) is oriented along the fiber while the two others (**a** and **b**) are randomly oriented around the fiber axis. This results in the typical fiber diffraction pattern of a flax fiber shown in Fig.6, which has rotational symmetry around the fiber axis.

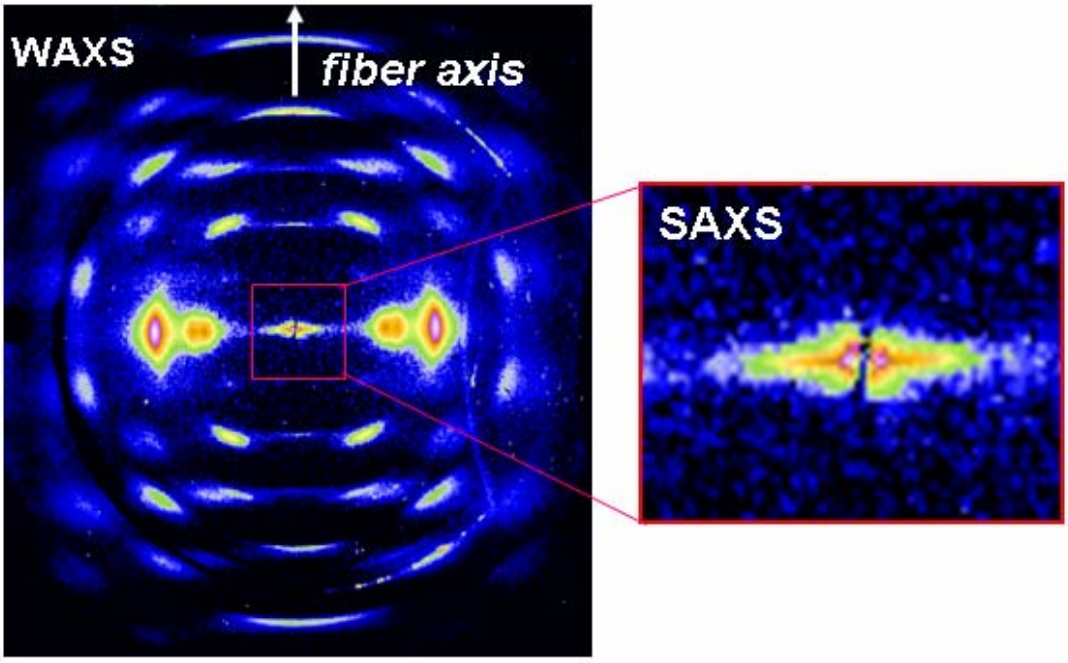

Fig.6 WAXS and SAXS diffraction patterns of a flax fiber after background subtraction. The WAXS pattern shows some diffuse scattering due to an amorphous fraction. The equatorial SAXS-streak is due to the electron density contrast between microfibrils and the surrounding lignin-matrix. This contrast can be increased by hydration [48].

The crystalline domains show an "orientation distribution" along the fiber axis, which can be derived from the azimuthal broadening of meridional or equatorial reflections [49].

3.3 Simulation of a cellulose fiber diffraction pattern

The simulation of cellulose fiber scattering was based on the software Cerius® (Accelerys), run on an ESRF Nice cluster. Fig.7 shows the generated reflection spots including Miller's indices for cellulose I_α using its published crystal structure [15].

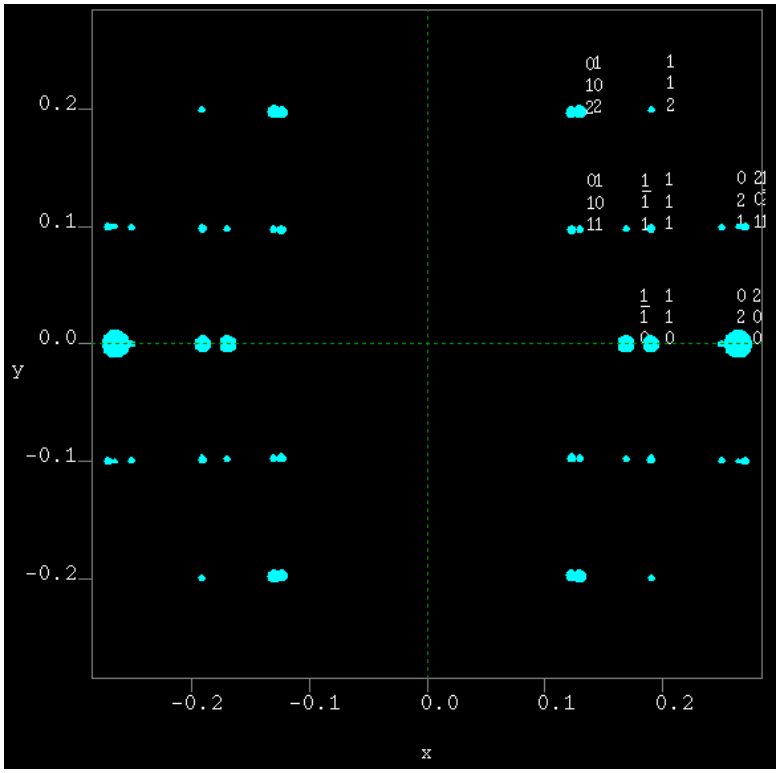

Fig.7 Simulated fiber pattern of cellulose fiber: λ=0.075 nm. The size of the spots is proportional to the reflection intensities. Miller's indices of the reflections are indicated. (Cerius® software)

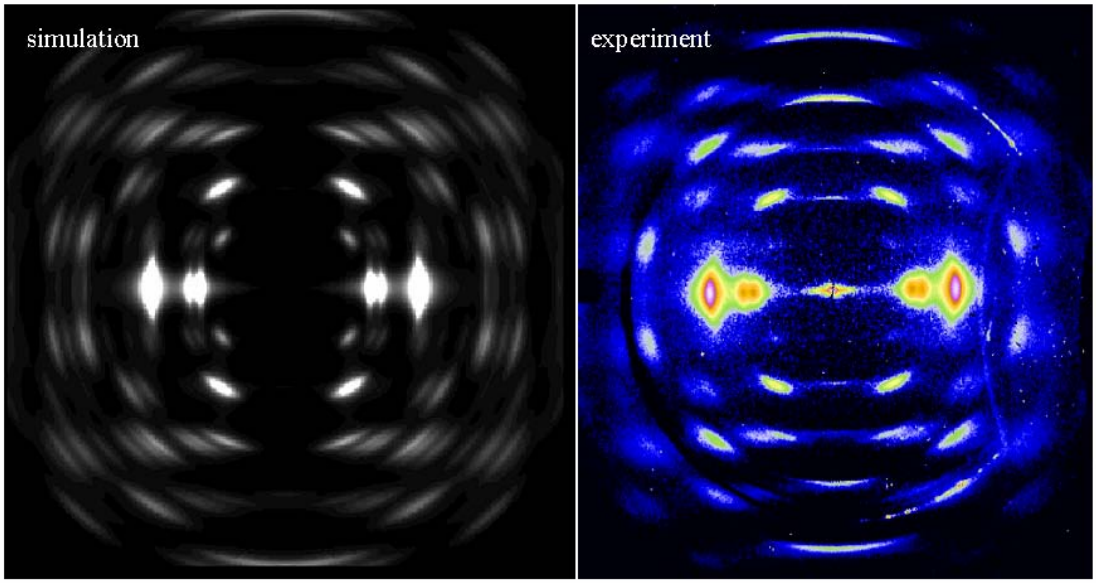

Fig.8 Comparison of simulated cellulose I_α fiber pattern (Cerius®) and experimentally observed fiber pattern from single flax fiber: λ=0.975 nm.

A more realistic simulation assuming a crystalline domain size of 10 nm along the three major axes and an angular spread of the domains along the fiber-axis with 5° fwhm shows a close resemblance with the fiber pattern from a flax fiber (Fig.8) and therefore consistence with the proposed crystallographic parameters of cellulose [13-15].

3.4 Introduction into microdiffraction

In order to spatially resolve details of a sample's microstructure by X-ray diffraction, one has to reduce the beam size in order to obtain local information (i.e. in a specific region of the sample). In this way, SAXS/WAXS techniques using a synchrotron microbeam have allowed to determine the local orientation in spherulites or to demonstrate skin-core effects [50]. The use of different kinds of optics to reduce the beam-size of the X-ray source allows two distinct classes of experiments: *single crystal microdiffraction* and *scanning microdiffraction* [4].

3.5 The ID13 microdiffraction beamline

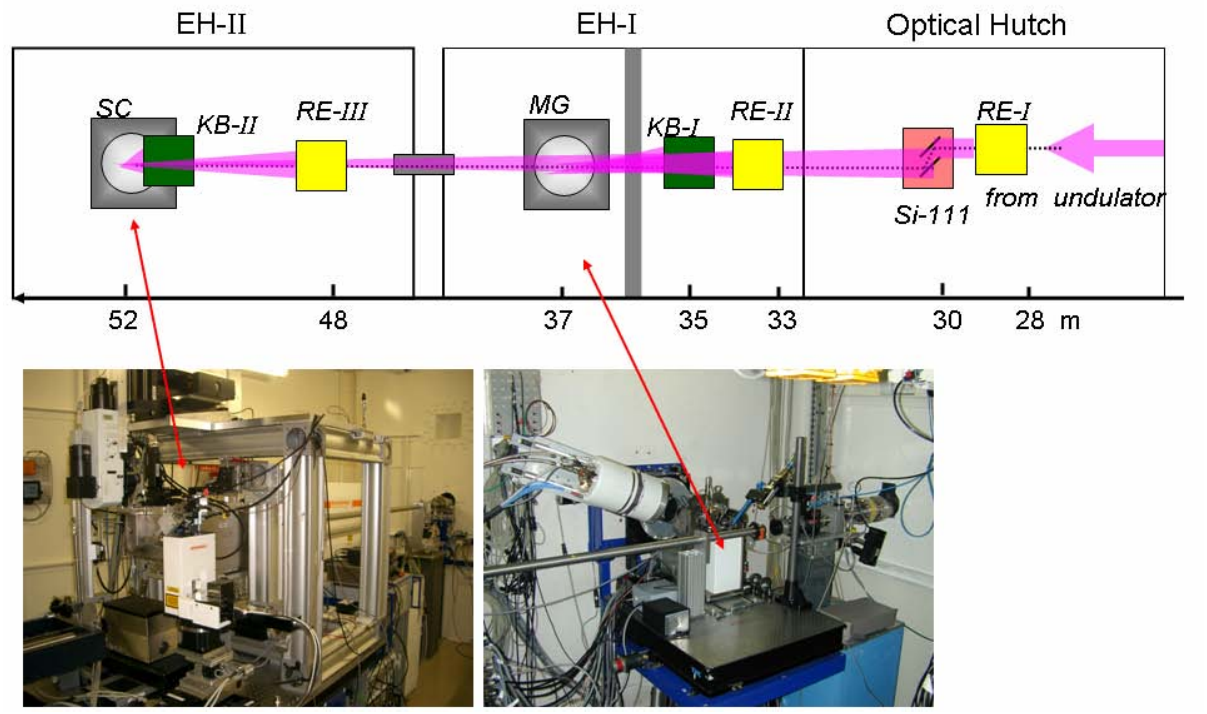

Fig.9 ESRF-ID13 hutches layout and images of hutches interior: RE-I/II/III: Be-refractive lenses at different focusing distances; Si-111: liq. N_2 cooled Si-111 monochromator; KB-I/II: Kirkpatrick-Baez mirrors for different focusing distances. A crossed Fresnel system was used instead of KB-II for the present experiments in EH-II. SC: scanning setup; MG: microgoniometer

The ESRF beamline currently provides beam sizes in the range of 30-0.1 µm. A low-β undulator is used as radiation source, which emits a line spectrum with a band width of the fundamental of $\Delta E/E \approx 0.02$. The position of the peaks can be tuned by modifying the undulator gap. A wavelength (λ) with a band width of $\Delta E/E \approx 0.0002$ is selected using a liquid N_2 cooled Si (111) double monochromator. For most polymer experiments a wavelength of λ = 0.097 nm is used, which corresponds to an energy $E = 1.24/\lambda$ of 12.78 keV.

Two experimental hutches are currently in use (Fig.9). The first (EH-I) houses a microgoniometer (MG), which is generally used for single crystal microdiffraction [51] and the second (EH-II) houses a scanning setup (SC) used for scanning microdiffraction [4]. The beam size at the source is 134_h x 25_v µm^2 (full-width at half maximum; fwhm) with a divergence of 2_h*0.2_v mrad^2 (h: horizontal; v: vertical). The focal spot at the microgoniometer is currently generated by a combination of prefocusing Be refractive lenses [52] and a 5 µm postcollimator in front of the sample [4]. The focal spot at the scanning set-up in the 2nd experimental hutch (EH-II) is generated either with similar Be-refractive lenses and postcollimator for a 5 µm beam or with crossed Fresnel lenses [53] providing a 300*300nm^2 beam.

4 Experimental methods

4.1 Materials

Experiments were performed with cotton fibers from a cotton flower[2] shown in Fig.10. The fibers were cleaned by refluxing in a mixture of ethanol and toluene (60/40 v/v) twice for four hours, in order to remove waxy components, and then air-dried. The cellulose purity should be close to 99% after this treatment [10]. Single fibers were selected with tweezers under an optical microscope and attached to specific sample supports.

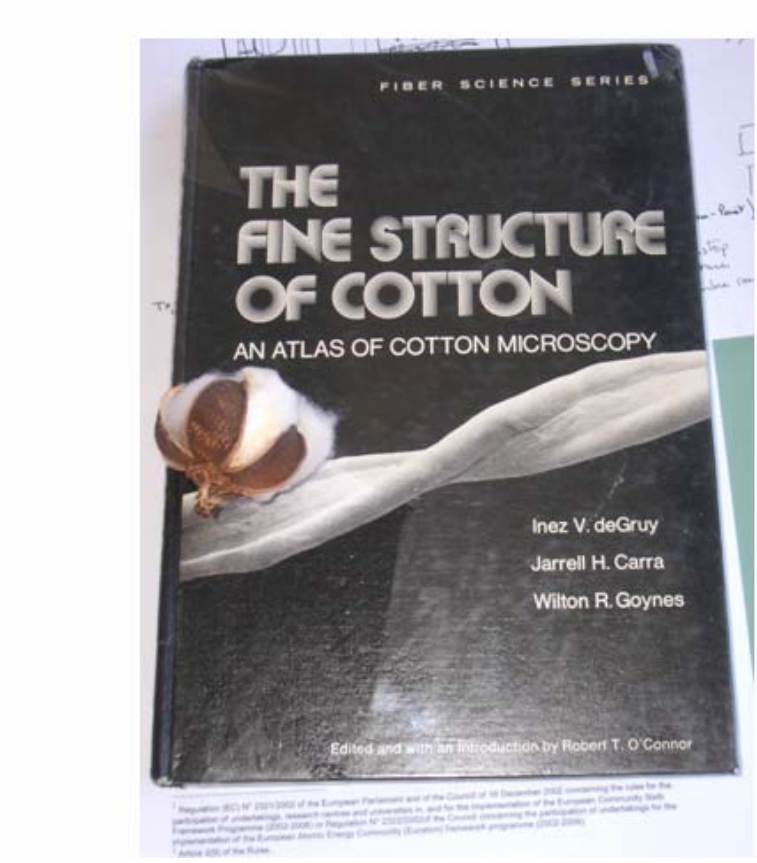

Fig.10 Cotton flower boll placed on a reference book on cotton microscopy [54].

In general, samples were kept under slight tension (0.4-0.8 g force) during the experiments using a stretching cell. (Section 2.3.2) This allowed maintaining the sample position for extended periods. Hydration experiments were performed by using demineralized water, which was applied to the cotton fibers by ejection from a microdrop generator at room temperature. (section 4.2.3)

[2] Gift from Dr. H. Chanzy, CERMAV-Grenoble

Soda treatment of the fibers was also executed with the microdrop generator at room temperature. The concentration of aqueous NaOH was 4 mass-% (= 1N), but due to the properties of the system – water can evaporate out of the fiber – the local concentration in the fiber was expected to vary up to substantially higher values. Some experiments were performed on fibers without tension. Fibers were submerged in aqueous NaOH solutions of 10 and 20 mass-% and glued to a glass capillary or a molybdenum ring by fast glue (Loctite®). For comparison, other aqueous alkali solutions were prepared using KOH, RbOH and CsOH salts[3]. The concentrations were 8N, 0.78N and 0.67N respectively. Aqueous $Sr(OH)_2$ solution of 0.05N was used for comparison with the alkali salts.

The alkali-cellulose samples were neutralized with 0.5N HCl when using the stretching cell and with 1N HCl for the capillary-mounted fibers. All solutions were microfiltered before insertion into the microdrop generator to avoid clogging (see also Annex A).

4.2 Instrumentation & sample environment

4.2.1 X-ray set-up

Experiments were performed using the two main diffraction set-ups at the ID13 beamline[4]. Single fibers of cotton -after reaction with aqueous NaOH or additional washing with HCl- were investigated using the microgoniometer in EH-I (Fig.9) [4]. Be-refractive lenses [52] were used as focusing element at a wavelength of the monochromatic beam of λ=0.097 nm. X-ray exposure of the sample was limited to the frame collection time by a fast shutter.

Scanning diffraction experiments were performed using the set-up installed in EH-II (Fig.9). These experiments were performed with crossed, linear Fresnel lenses [53] at a wavelength of λ=0.097 nm (Fig.11).

[3] CsOH and RbOH were kindly provided by Dr. Olivier Diat, CEA-DRF

[4] Installation and alignment of optical system was performed by beamline staff and in particular by Dr. M. Burghammer

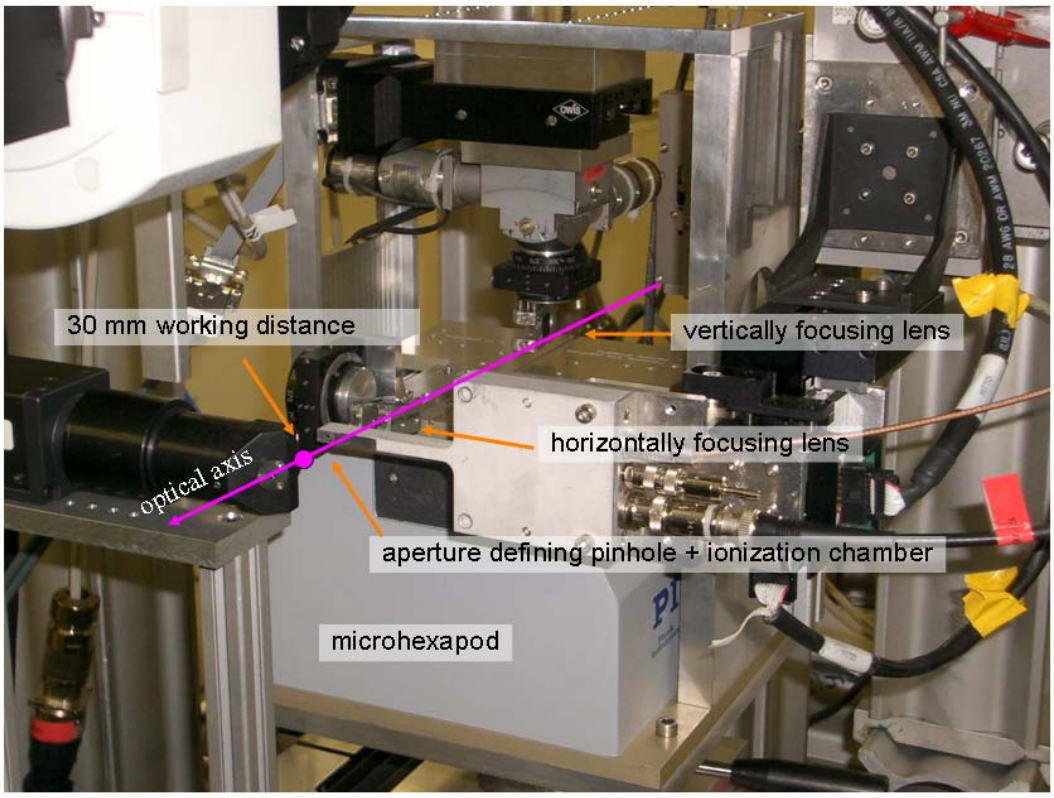

Fig.11 Fresnel set-up showing the optical elements and the available working space. The microhexapod structure is used for aligning the horizontally focusing Fresnel lens relative to the unfocused beam. The vertically focusing lens is aligned using a motorized goniometer stage.

Diffraction patterns were recorded with a slow-readout CCD detector (MAR CCD), which has a GdO_2S_2 X-ray converter screen of about 165 mm diameter. The X-ray converter is connected by a tapered fiber-optics to a 2K*2K CCD chip. Full, 16-bit pattern readout/storage takes about 12 seconds. In the following the term “frame” will be used for the sum of data collection and readout/storage time. By binning to 1K*1K the readout/storage time can be reduced to about 3 sec. This option was used for most in-situ experiments. The sample-to-detector distance was calibrated by an Al_2O_3 standard powder.

4.2.2 Stretching cell

The stretching cell (Fig.12) used for the experiments was originally developed at the University of Manchester in the group of Prof. R. Young [55]. Single cotton fibers were glued to cardboard frames, which were glued to the stretching cell support elements. A load cell allowed measuring the stress curve. During experiments, the fibers were kept at a fixed stress.

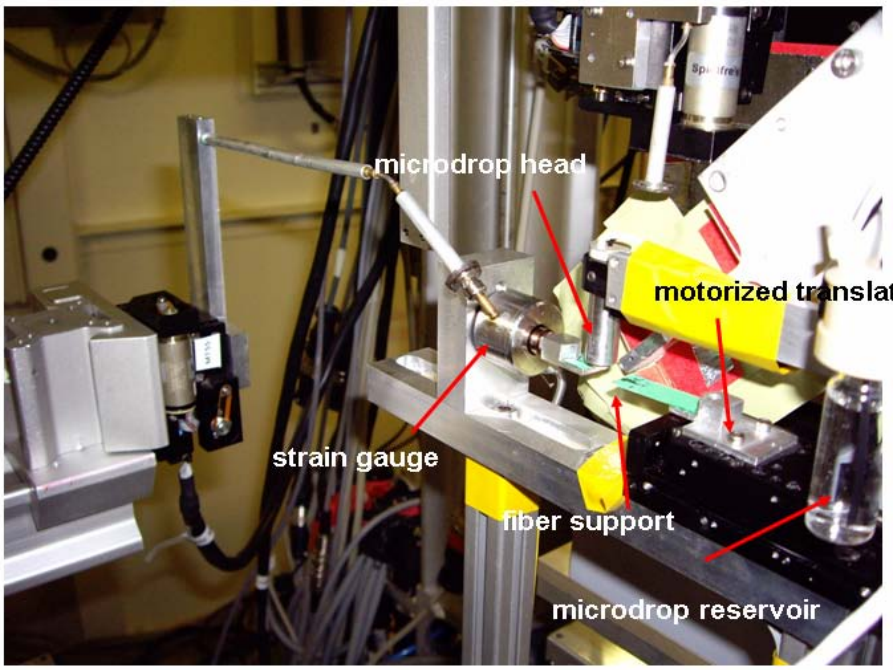

Fig.12 Picture of stretching cell and microdrop generator installed at the ID13 beamline.

4.2.3 Microdrop generator

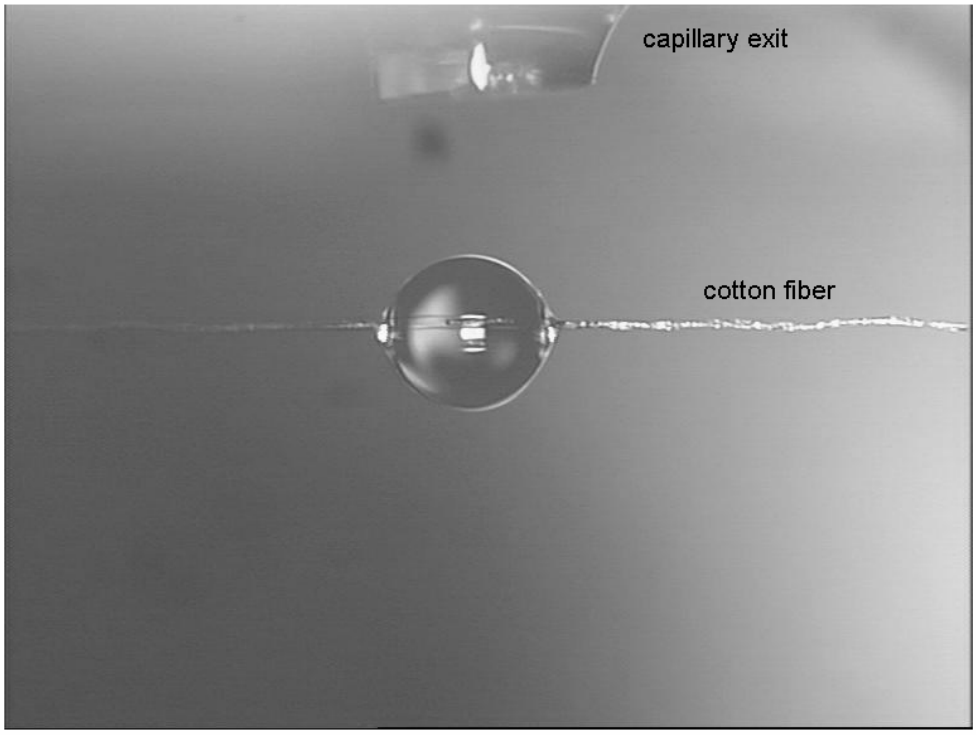

Fig.13 Generation of an aqueous NaOH "macrodrop" on a cotton fiber. The macrodrop is maintained at equilibrium size limited by water evaporation and aqueous NaOH diffusion into the fiber. The distance of the capillary exit from the fiber is about 400 μm. The diameter of the droplet in the fiber direction is 300 μm. A droplet frequency of about 1 Hz was applied. The droplet is maintained on the fiber by surface tension.

For in-situ reaction with water, water microdrops (called also "droplets") generated by a drop-on-demand system[5] were used [6, 56] (Fig.12). The system is based on a glass capillary mounted concentrically in a piezoelectric actuator, which implies that droplets are not heated during ejection. It was also possible to eject alkaline or acid droplet. The droplet diameter is defined by the capillary exit to about 50 μm with a relative change in volume of consecutive microdrops of ±1% (company specs). For such diameters, the surface energy will dominate with respect to kinetic energy and droplets will not splash when hitting the fiber. Fig.13 shows the microdrop generator head installed above the fiber, which is fixed to the stretching cell. The distance of the capillary exit to the surface of the fiber varied from 300-400 μm.

[5] Microdrop, Norderstedt, Germany; www.microdrop.de

A droplet frequency of a ≤1Hz allowed maintaining a constant liquid supply at the sample position. This results in the generation of a “macrodrop” on the fiber (Fig.13). The control unit of the system was triggered by a TTL signal from a VME frequency generator board. Software control was possible through a SPEC interface running on a UNIX based workstation (Certified Scientific Software; see also Annex B).

4.3 Data calibration and analysis

4.3.1 Data calibration

The detector-to-sample distance was determined from the position of selected powder rings of Al_2O_3 on the detector, the pixel size of the detector (MARCCD: 78.94*78.94 μm^2), the d-spacings of the reflections and the wavelength using Bragg's equation (Fig.14). The position of peaks was determined by FIT2D [57].

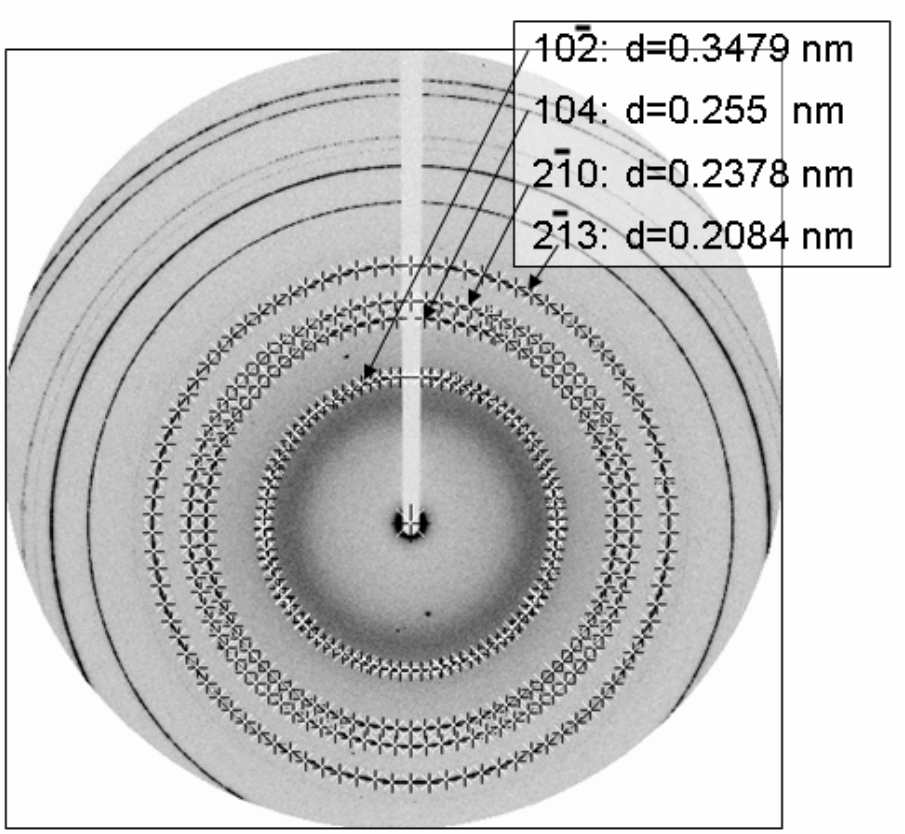

Fig.14 Diffraction pattern from standard Al_2O_3 powder with selected powder rings fitted by FIT2D [57].[6] Miller's indices of selected reflections and d-spacings are indicated.

[6] www.esrf.fr/UsersAndScience/Experiments/SCMatter/ID13/handbook/calibration/Al2O3

4.3.2 Analysis of individual patterns and sequences of patterns

Individual patterns were displayed and analyzed using the software package FIT2D [57]. For background reduction a pattern recorded outside the sample area was subtracted. Negative spikes in the background-subtracted patterns were masked prior to curve fitting. These negative spikes can be due cosmic radiation or due to scattering from beamstop or aperture edges.

A polymer fiber pattern is shown schematically in Fig.15.A [4, 58]. The numbers indicated in Fig.15.A and table I indicate the main information, which can be extracted using FIT2D.

(1)	Bragg spacing	crystal parameter and strain
(2)	azimuthal profile	integrated intensity, orientation distribution
(3)	radial profile	integrated intensity, particle size
(4)	background scattering	amorphous content

Table I Peak profile parameters, which can be derived using FIT2D

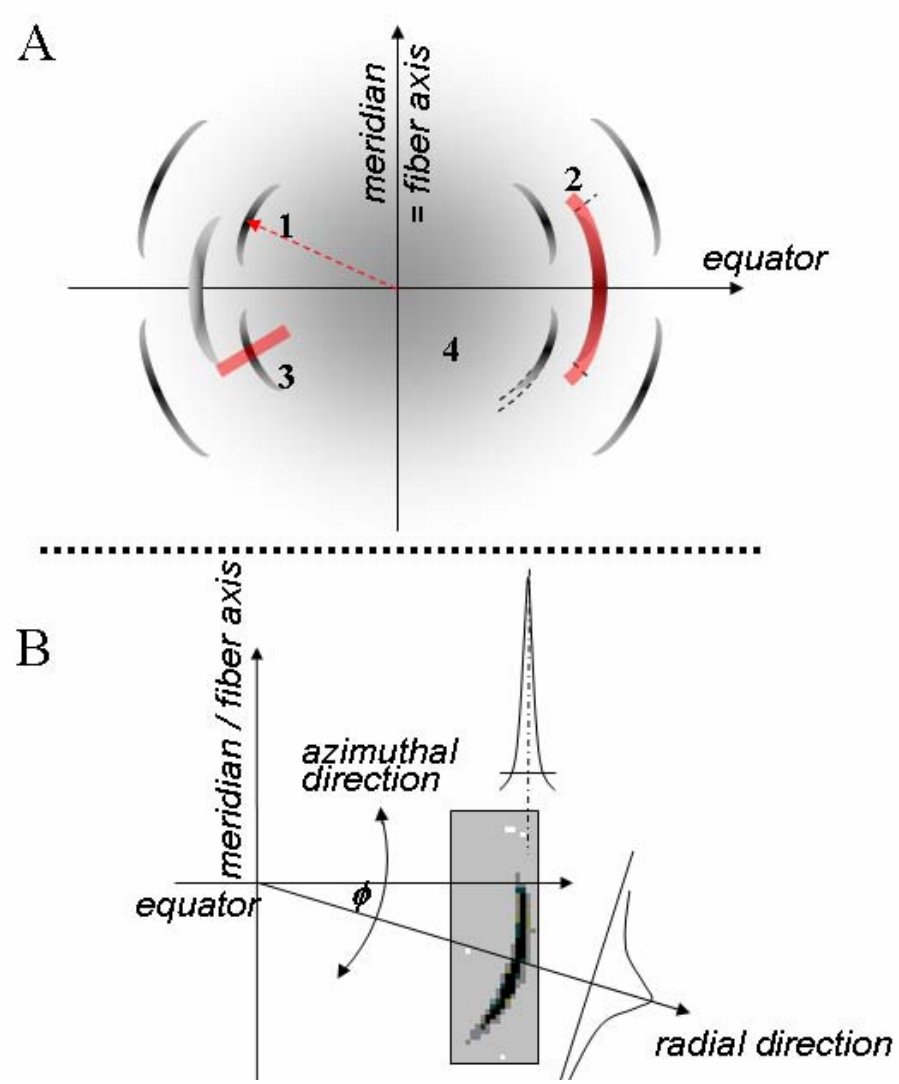

Fig.15 A: schematic fiber diffraction pattern with numbers indicating specific information, which can be obtained during data analysis; B: schematic display of a peak, which is rotated by an angle ϕ against the equator. The profiles in radial and azimuthal directions are indicated [4]. The meridian is oriented along and the equator normal to the fiber axis.

Fig.15.B shows schematically azimuthal and radial profile fits. The ϕ-parameter, which indicates the orientation of the local fiber axis, can also be extracted.

For recursive data analysis, a batch processing software developed by R. Davies was used [59]. This allows extracting the parameters indicated in Table I from consecutive files of a mesh-scan. A composite image of the mesh-scan with a specific parameter provides a visual information on the distribution of a specific feature [4].

5 Results & discussion[7]

5.1 Basic structures

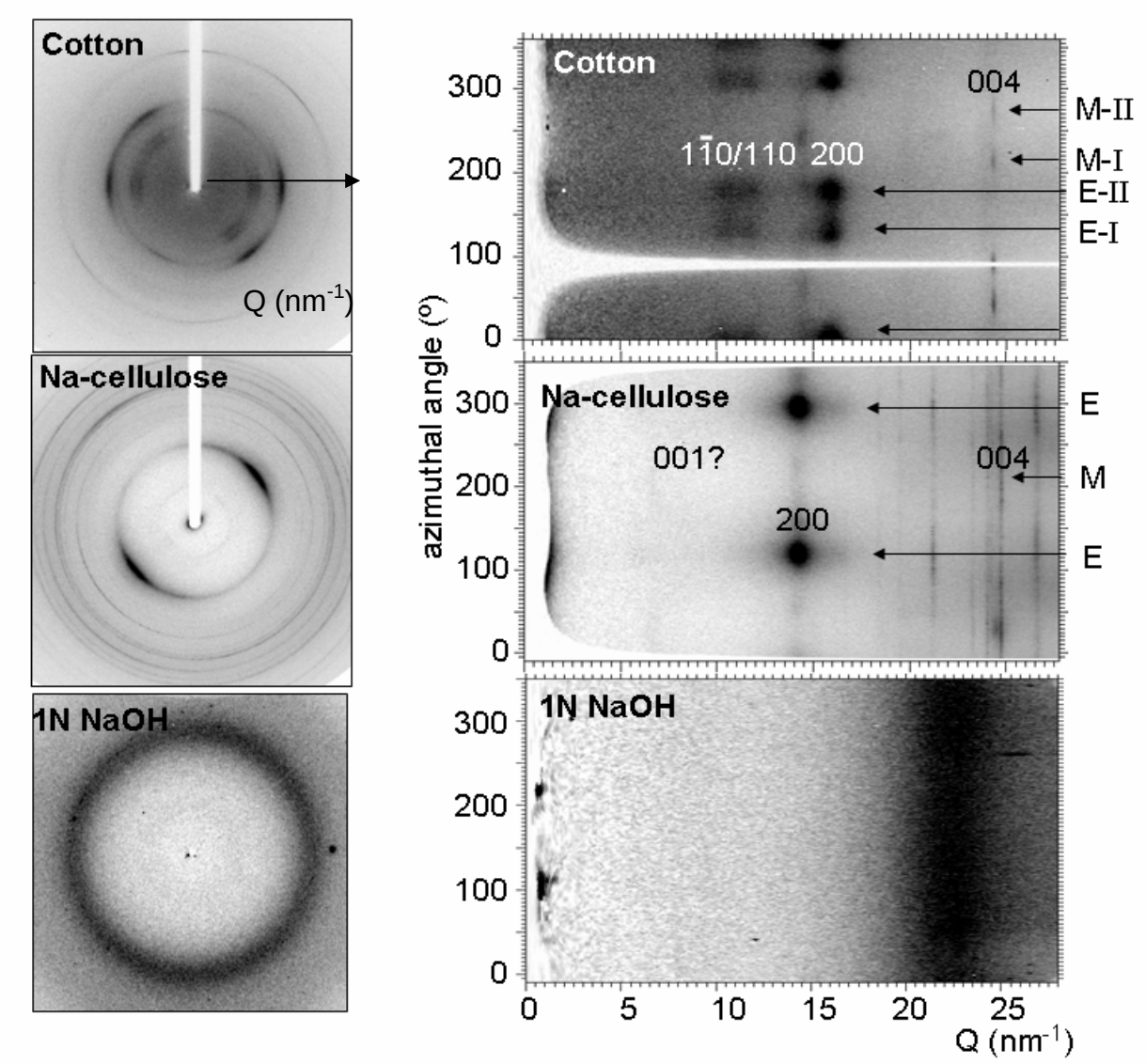

Fig.16 Diffraction patterns of cotton (cellulose I), Na-cellulose and from within an aqueous NaOH macrodrop. The patterns from cellulose I and Na-cellulose were recorded with the ID13 microgoniometer and the aqueous NaOH pattern with the scanning set-up (section 3.5). The cotton fiber shows split equators (E) and meridians (M); see also Fig.15. Miller's indices: cellulose [60, 61]; Na-cellulose [3]. Note the weak 001 reflection of Na-cellulose, which does not fit to the published Na-cellulose reflections [2].

[7] Scans are numbered by consecutive numbers (Scan 1…Scan n) in the text and assigned to file names in Annex C. For all following scan-experiments, the fiber axis was horizontally. A mesh scan $15_h*5_v\mu m^2$ implies that the steps along the horizontal fiber axis between two consecutive diffraction patterns were 15 microns horizontally and 5 microns vertically.

In order to interpret the structural processes during the chemical transformation, diffraction patterns of the basic structures before and after reaction were collected at 300K using the microgoniometer and a 5_h*5_v μm^2 beam. In addition a pattern from an aqueous NaOH macrodroplet was collected using the scanning diffraction setup and a 300_h*300_v nm^2 beam (Fig.16). The diffraction pattern of the cotton fiber shows split equators (E-I/E-II) and meridians (M-I/M-II) of cellulose I due to the helicoidal structure of the macroscopic cotton fiber shown in Fig.10. Note that the meridian peaks are very weak in intensity. After reaction to Na-cellulose, the helicoidal structure has disappeared. The indexation of the strongest cellulose I reflections is based on: [60, 61] and that of Na-cellulose on: [3]. We note a weak reflection at the 001 reflection position, which is not allowed for the orthorhombic Na-cellulose I unit cell [15]. The possible existence of a fraction of other Na-cellulose phases [2] will have to be investigated in more details as the concentration of NaOH has likely increased up to saturation level (see below).

5.2 Cotton hydration

Hydration experiments were performed to determine the extent of diffusion of water into the fiber, which is of interest to compare with the spatial distribution of Na-cellulose in the fiber.

A single cotton fiber was hydrated by H_2O microdrops until the macrodrop on the fiber had reached a constant size of 150_h*115_v μm^2. Hydration was stopped and a mesh-scan with the 300_h*300_v nm^2 Fresnel beam (section 4.2.1) was started immediately, centered around the droplet centre with $\pm$ 100 μm range and a mesh resolution of 5_h*5_v μm^2.[8] The measuring time/pattern was 1 sec for a binned MARCCD detector with about 3 sec readout time (for processing the data and saving it to the server's hard disk). The total data collection time of 287 frames was about 19 min. A zoom of a single pattern (Fig.17.A) shows a split equatorial 200 cellulose reflection and an increase of SAXS scattering close to the beamstop. The increase of SAXS scattering during hydration is assumed to be due to an increase of electron density contrast between microfibrils and matrix [48].

[8] Scan 1; see Annex C

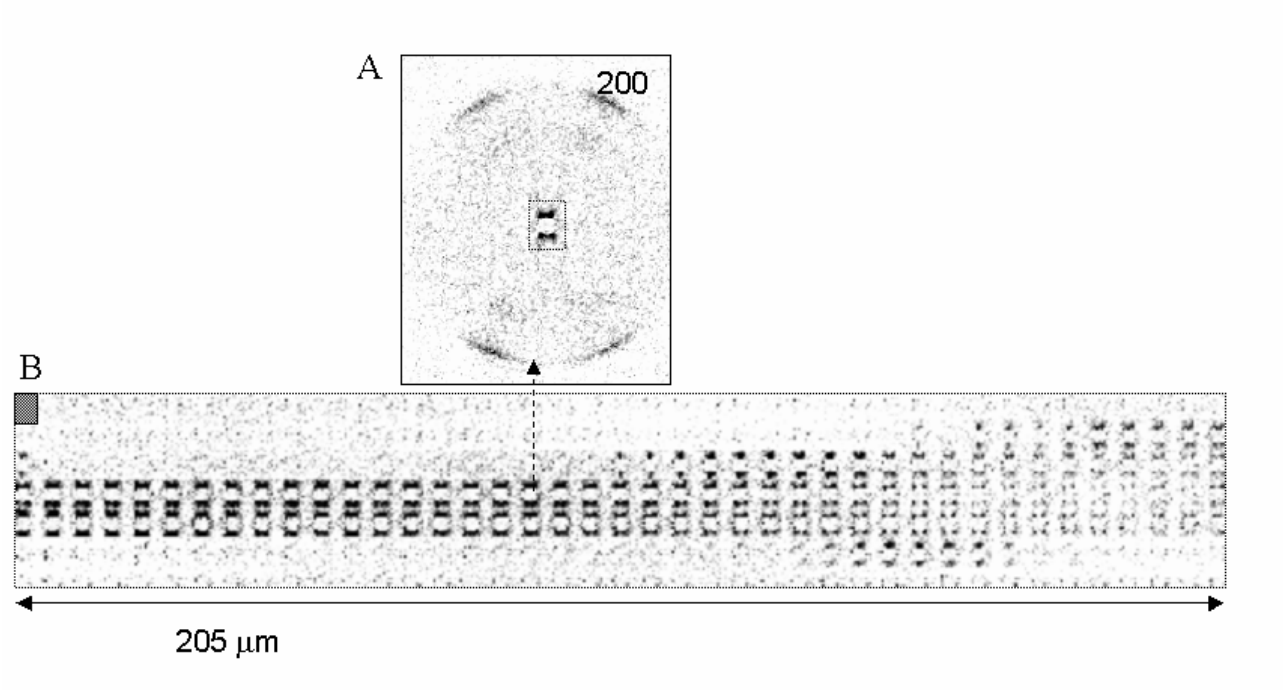

*Fig.17 A: zoom of WAXS pattern of hydrated cotton fiber from within the macrodrop zone; B: composite image of "pixels" from the central SAXS area across the mesh-scanned area of the fiber. The step-width of the mesh was 5_h*5_v μm^2.The H_2O diffusion along the fiber shows clearly.*

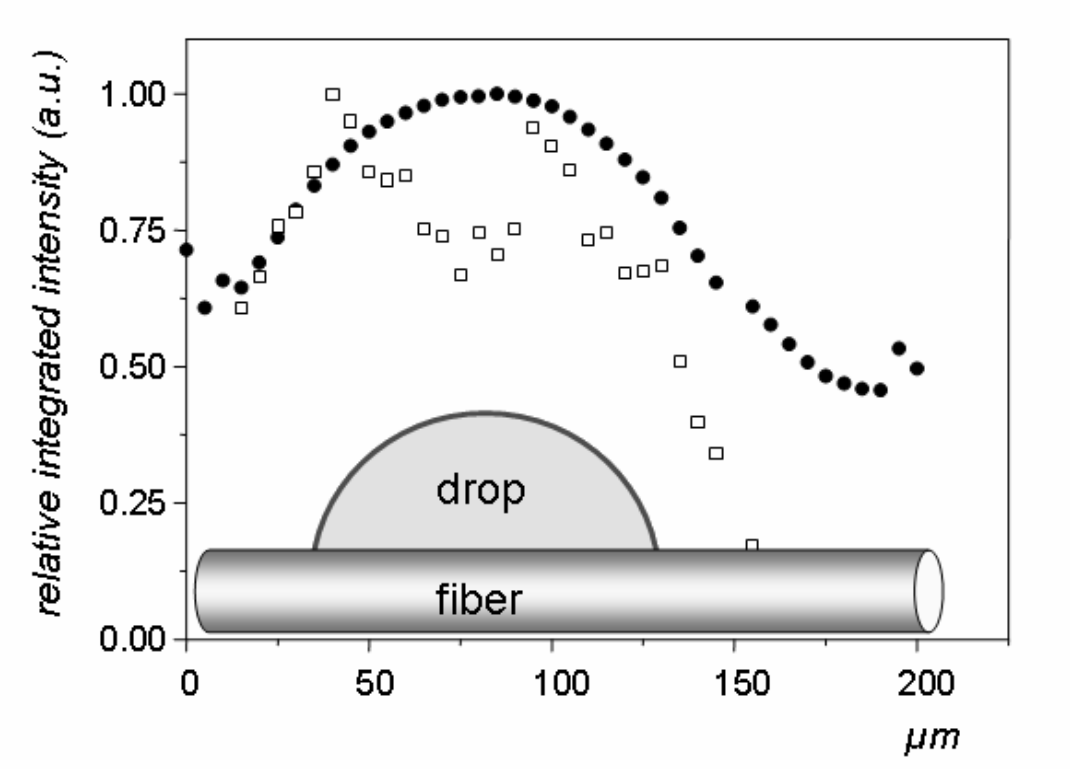

Fig.18 Variation of integrated SAXS intensity (open squares), when scanning the macrodrop (see also Fig. 17.B). Variation of integrated intensity of liquid (NaOH(aq.)) scattering peak (filled circles; WAXS) determined just outside the fiber. The maximum at ~75µm marks the center of the macrodrop. SAXS and WAXS yield approximately the same results for H_2O distribution.

This can be seen qualitatively from the composite picture containing only the central SAXS area in every pattern (Fig.17.B). The figure shows a decrease of SAXS intensity to the edge of the fiber. The twisting of the fiber along the macroscopic fiber axis (Fig.10) can be readily discerned from the composite image.

For a more quantitative analysis, the patterns containing scattering information were summed normal to the fiber axis in order to increase the counting statistics. This allowed determining the variation of the integrated SAXS intensity in the central part close to the beamstop across the macrodrop (Fig.18). In practice the intensities were integrated in the central part, excluding a circular area around the beamstop. Background scattering was not subtracted. For comparison the spatial extent of liquid scattering was determined by integrating the liquid scattering peak, which is for H_2O similar to the 1N NaOH peak shown in Fig.16. For this the complete azimuthal range of the liquid scattering ring was integrated for all patterns, again without subtraction of an underground. Both intensity distributions (scaled individually to 1 at max. intensity) are quite similar, which suggests that the increase in SAXS-intensity is confined to the range of the macrodrop.

5.3 Formation of sodium-cellulose

The swelling with 1N aqueous NaOH microdrops was studied in the same way as water hydration. This NaOH concentration is below the limit of the structural change reaction of cotton fibers [62] but it was expected that the concentration in the fiber would increase due to evaporation. Microdrops were generated at a frequency of ½ to 1 Hz and accumulated within a macrodrop on the fiber. The extent of reaction can easily be visualized by FIT2D in the form of a composite image as already shown for the hydration process (Fig.17).

Thus Fig.19 shows a composite image using “pixels” corresponding to the zoomed area shown in Fig.17.A.[9] The extension of the fiber from the zone dominated by liquid scattering (Fig.16) can directly be visualized. Selected individual patterns

[9] Scan 3; see Annex C

clearly show the transition from the split cellulose I pattern to the Na-cellulose pattern[10] (see also Fig.16).

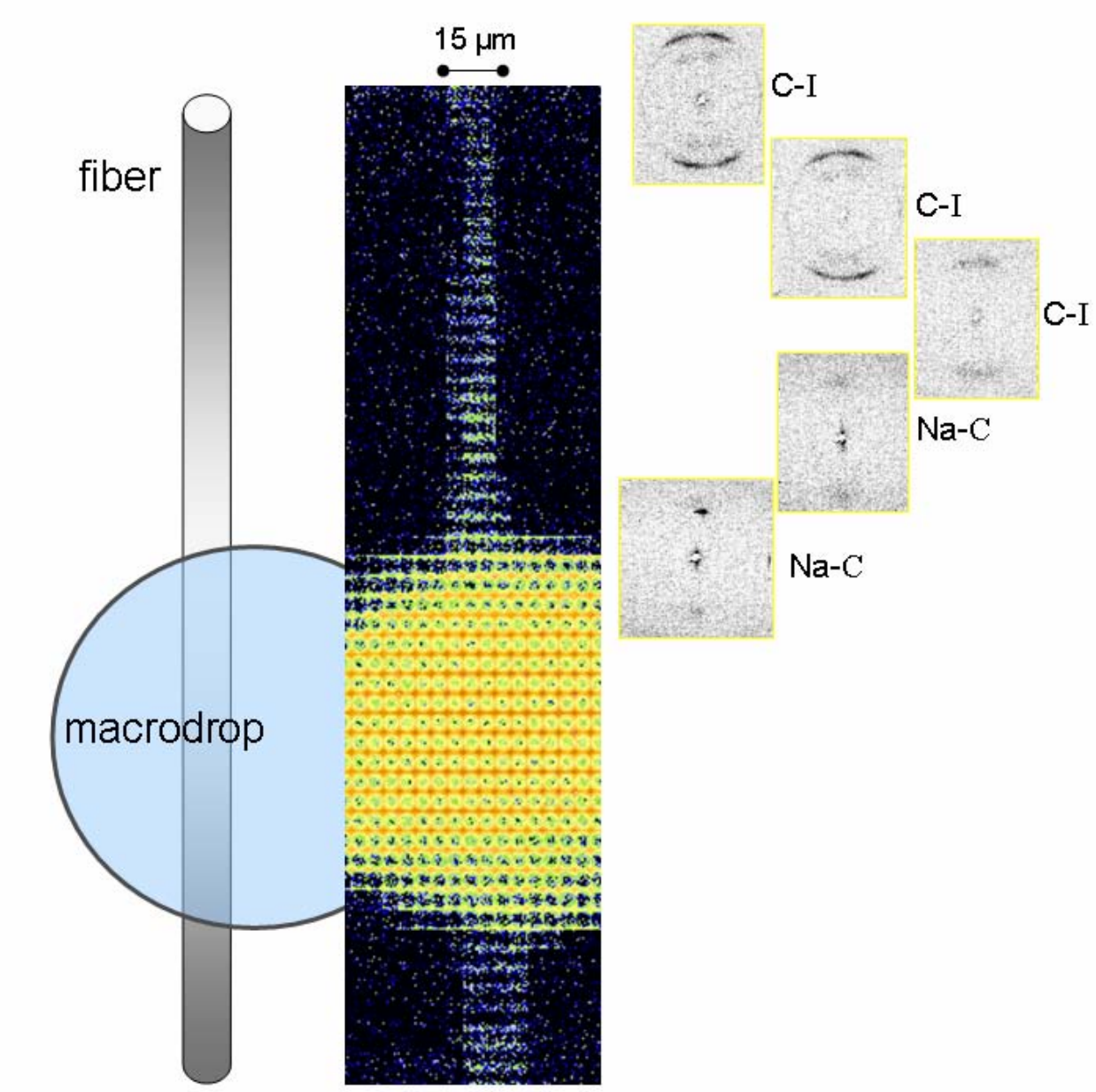

Fig.19 Composite image based on "pixels" containing the area of the strongest equatorial peaks in cellulose I, Na-cellulose and of liquid scattering background (Fig.16). The spatial extensions of the fiber and the "macrodrop" are visible. Selected "pixels" are highlighted at the right. Abbrev.: C-I: cellulose I; Na-C: Na-cellulose. The intensities of the Na-cellulose peaks are relatively weak, as the hydrated NaOH containing macrodrop generated in the previous experiment[11] has been "washed" with H_2O microdrops prior to the present experiment[12].

[10] It will be assumed that Na-cellulose I is initially formed due to the initially low NaOH concentration [2].

[11] Scan 2; Annex C

[12] Scan 3; Annex C

This shows qualitatively that the spatial extension of the Na-cellulose formation is well beyond the extension of the macrodrop. One also observes an equatorial SAXS streak (intensity in the center of the diffraction pattern, surrounding the beamstop) for the Na-cellulose patterns, which could be related to the suggested decrease in void volume during swelling of cellulose fibers [36].

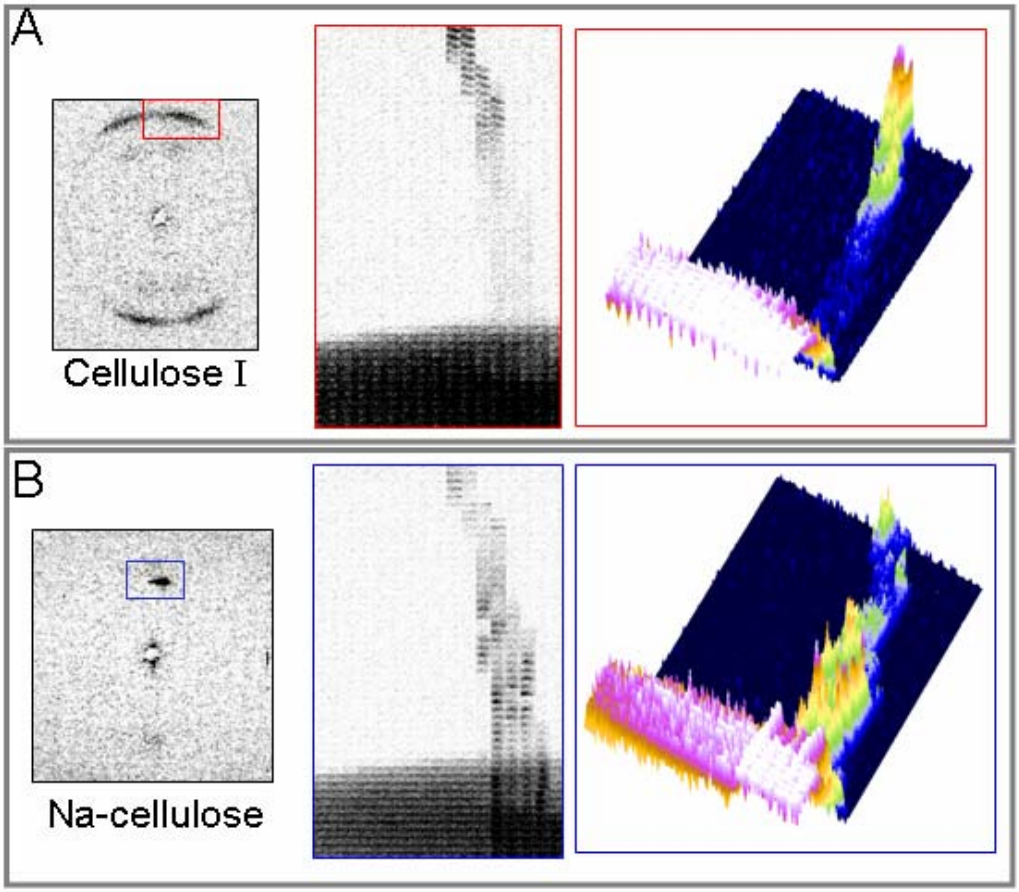

Fig.20 A: composite image based on pixels corresponding to 200 reflection of cellulose I. Both projections and pseudo-3D displays are shown;[13] B: same for 120/200 reflections of Na-cellulose after reaction with NaOH droplets.[14] Note the different peak characteristics.

A more selective display is possible based on an area covering as closely as possible selected reflections. This is shown for the strongest equatorial reflections of cellulose I and Na-cellulose in Fig.20. The spatial extent of cellulose I and Na-cellulose scattering can thus easily be discerned, in particular from the pseudo-3D plots. One can even visualize the fiber "entering" the macrodrop.

[13] Scan 2; Annex C
[14] Scan 3; Annex C

We will now analyze two consecutive mesh scans on a cotton fiber, which was first exposed to 1N NaOH droplets (Scan 3) and then to H_2O droplets (Scan2). The aim was investigating the influence of such a dilution on the Na-cellulose phase in the fiber. Dropping of 1N NaOH droplets was maintained for about 160-170 sec until the size of the macrodrop had reached a constant value of about 300 µm and equilibrium between diffusion, reaction and evaporation had been reached. Microdrop generation was then stopped and the scan started for an area of 750_h*80_v μm^2 with a mesh width of 15_h*5_v μm^2 and 0.5 sec/pattern. The horizontal scan started at 750 µm from the macrodrop centre. It was not possible to reduce the step width in the mesh-scan or to increase the exposure time as the radiation damage resulted in a frequent breaking of the fiber. A total of 867 frames were collected corresponding to an overall data collection time of about 51 min. The volume of the macrodrop was reduced during this period due to water evaporation by only about 5%.

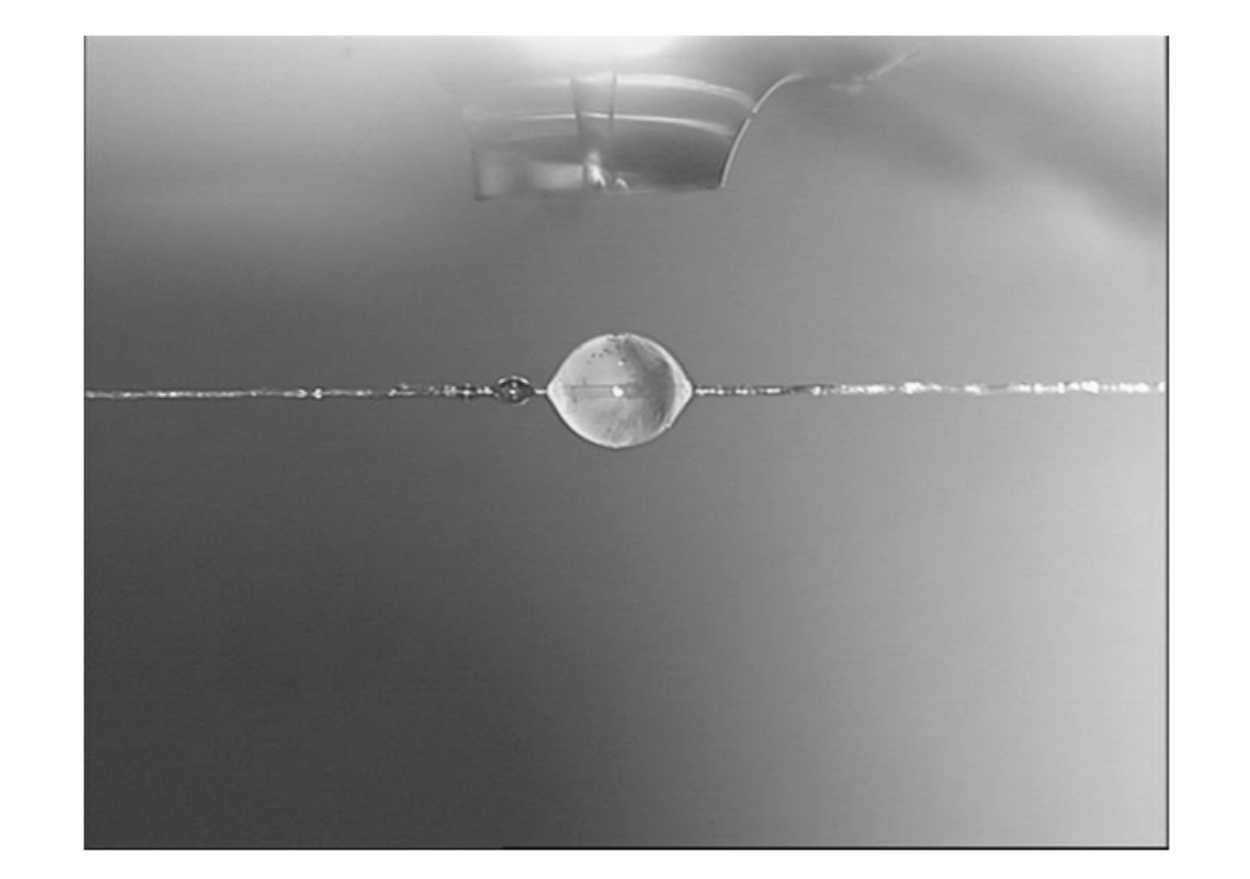

Fig.21 Macrodrop with formation of solid NaOHH_2O on its surface (compare with Fig.13).*

This resulted in an increase in NaOH concentration until solid NaOH*H_2O precipitated at the surface of the macrodrop with a characteristic light blue color.

(Fig.21) Precipitation of white $NaOH*H_2O$ crystals was also observed within the macrodrop, suggesting that the NaOH concentration had reached the limits in solubility of NaOH in H_2O of about 107 mass-% [63].

A second, identical mesh scan was performed after dropping H_2O microdrops for about 30 min on the alkaline macrodrop. The scan was again started after microdrop generation had been stopped. In contrast to the previous scan, the horizontal scan range of 750 µm was, however, displaced so that the whole macrodrop could be covered.

For quantitative analysis, patterns in rows normal to the fiber axis containing a diffraction pattern were summed in order to obtain a better intensity statistics. The individual patterns were then azimuthally averaged and the sequence of 1D powder patterns was plotted in projection. Fig.22.A-left shows a composite image of a 15_h*5_v μm^2 mesh corresponding to the reaction of the cotton fiber with 4% aqueous NaOH microdrops. The zoom area of an individual "pixel" is shown in Fig.17.A. The intensity sequence is shown in Fig.22.A-right. After washing of the macrodrop with H_2O droplets for about 30 min and a second mesh-scan (same mesh-size but displaced along the fiber), the composite image and intensity sequence of Fig.17.B-left/right was obtained.

The data suggest that the Na-cellulose peak becomes weaker upon washing with H_2O, which implies that part of the Na-cellulose has been transformed either back into cellulose I or into cellulose II (see Fig.22). It can also be seen qualitatively that the cellulose peak in the H_2O washed fiber extends closer to the macrodrop as for the same fiber, which had been reacted before with aqueous NaOH. There is, however, no evidence for cellulose II reflections [39, 64]. The strong reflections in the range $20<Q<30$ nm^{-1} seems rather to belong to a $NaOH*H_2O$ phase [65, 66]. This might be due to the fact that the washing process takes place in the closed environment of a fiber where a dilution is compensated eventually by evaporation.

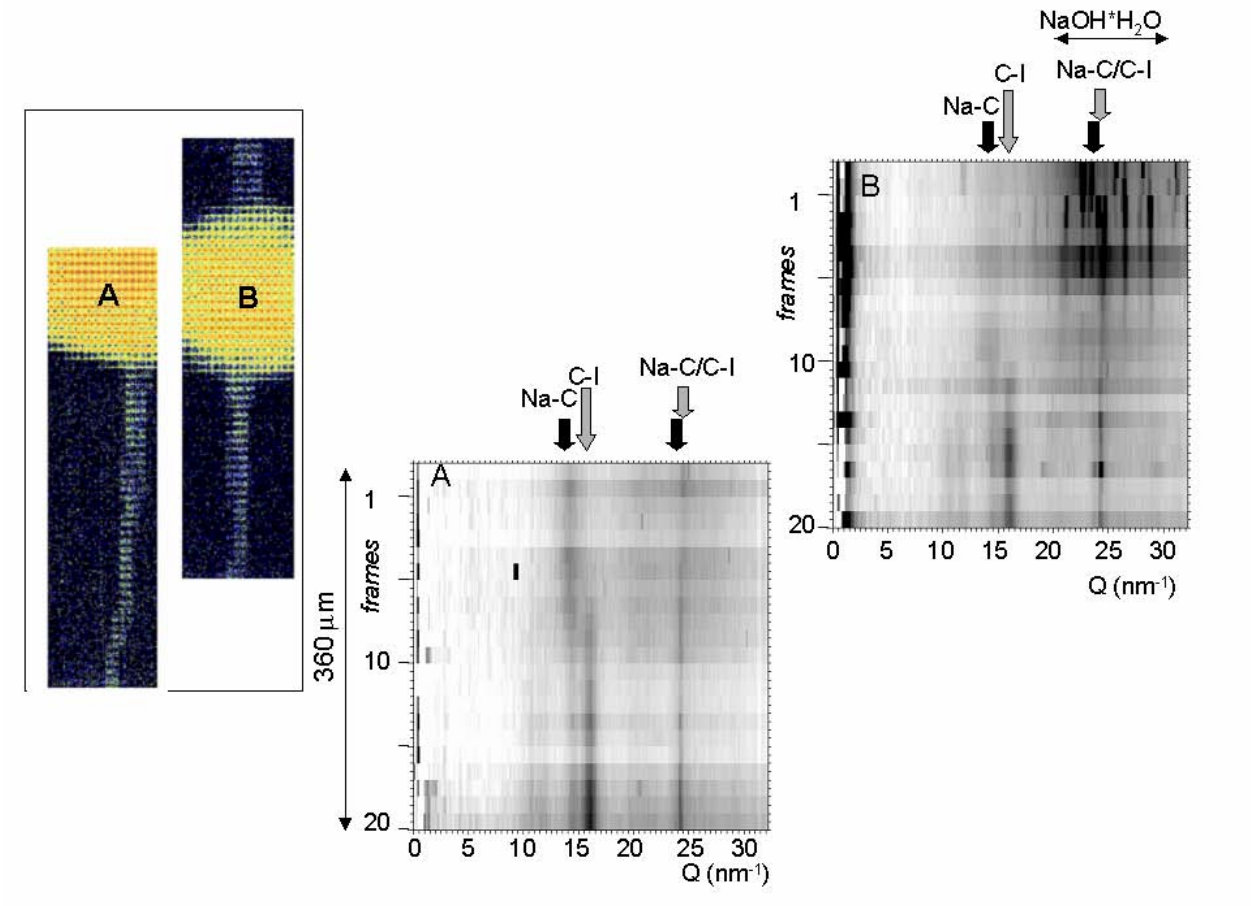

Fig.22 A-left: composite image of a fiber reacted with aqueous NaOH in a $15_h*5_v\mu m^2$ mesh. The "pixels" correspond to Fig.17.A; B-left: same but after "washing" the macrodrop with H_2O microdrops. A-right: projection sequence of cake-regrouped patterns; B-right: same but after "washing" macrodrop with H_2O microdrops. The positions of the strongest reflections of the different phases are indicated. The scanned zones along the fiber differ in both cases. The two patterns have therefore been vertically displaced so that the scanned zones match. Note that the scale of the patterns in A/B-left do not match with A/B-right.

There is evidence that the transition zone Na-cellulose to cellulose I is shifted during H_2O washing toward the macrodrop. This is shown in Fig.23 for two consecutive mesh-scans with NaOH microdrops[15] and H_2O microdrops[16]. Note that the mesh-size ($15_h*3.5_v$ µm^2) and the upper end of the fiber were identical for both scans. This allows deducing a shift of the cellulose I to Na-cellulose phase-limit by 225 µm towards the macrodrop centre.

[15] Scan 4; Annex C
[16] Scan 5; Annex C

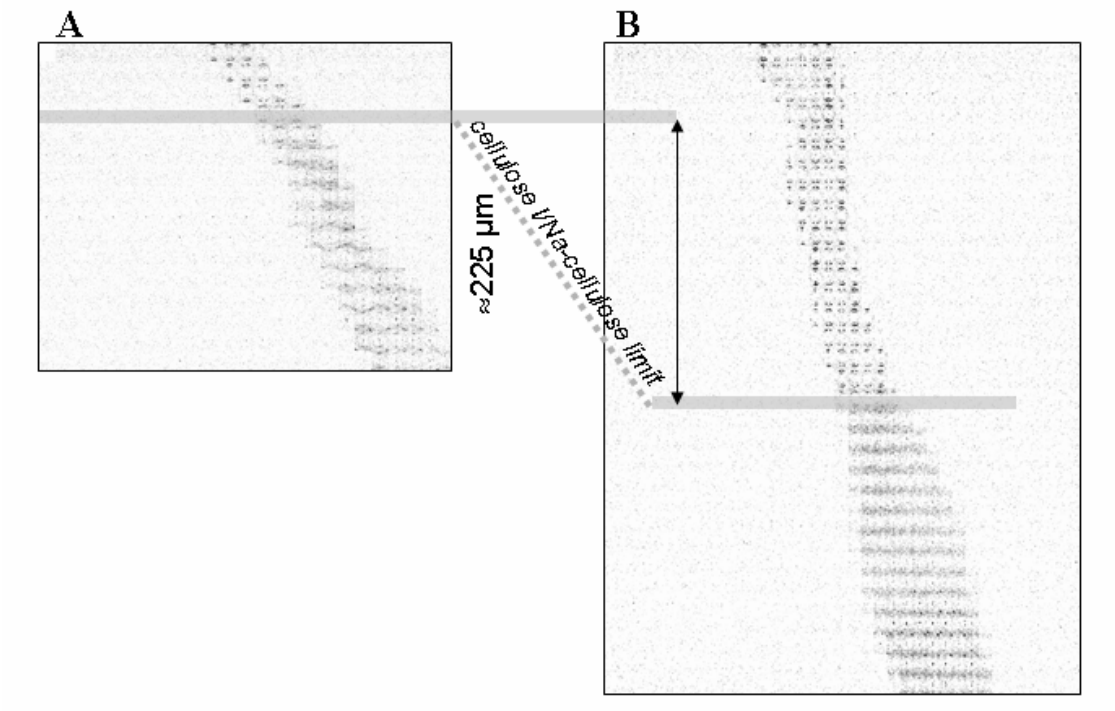

*Fig.23 Variation of position of transition zone Na-cellulose to cellulose I; A: after reacting by aqueous NaOH microdrops; B: after washing with H_2O microdrops. Mesh-size of both scans: 15_h*3.5_v μm^2, A cropped due to lateral switch of fiber (whole length was scanned as in B).*

This seems supporting the assumption of two types of Na-cellulose I [64, 67], which were suggested to be a "bent form Na-cellulose I_I" (reversible) and a "bent-twisted Na-cellulose I_{II}" (irreversible) [67]. Only Na-cellulose I_I can be transformed back to cellulose I according to these authors. Whether these conformational differences exist cannot, however, be deduced from the present data.

We will now consider in more detail the evolution of peak parameters during the cellulose I/Na-cellulose transition. The analysis will be based on the Na-cellulose 004 reflection using Gaussian profile fits.[17] Thus the evolution of the peak position is shown in Fig.24.

[17] Scan 2; Annex C; The patterns containing diffraction intensity in every vertical row (normal to the fiber axis) were summed in order to obtain a better counting statistics.

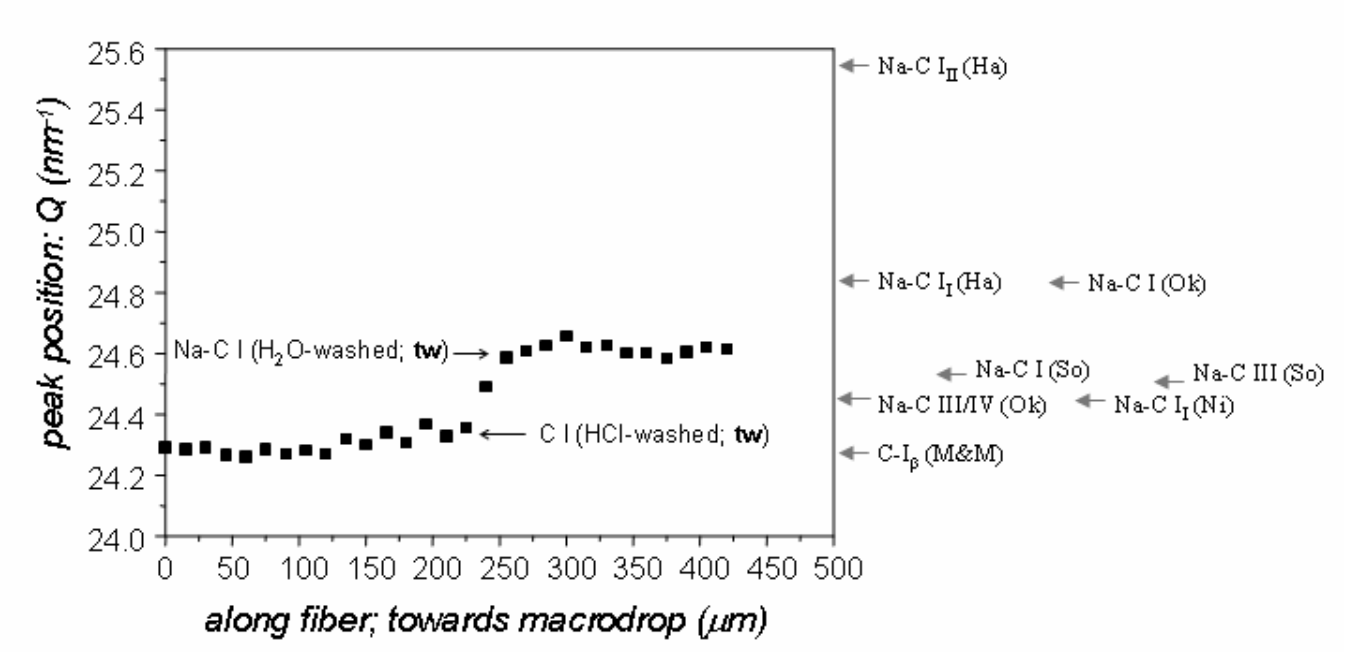

*Fig.24 Evolution of peak position across transformation zone from Na-cellulose to cellulose I. The scan extends to the edge of the macrodrop. Abbreviations: Na-C I: Na-cellulose; C-I: Cellulose I; References: **tw**: this work; Ha [67]; M&M [61]; Ni [3]; Ok [1]; So [62].*

The comparison with literature values of various Na-cellulose peak positions shows a large variability. One notes in particular the large positional difference of Na-cellulose I_I and Na-cellulose I_{II} peak positions [67], which is not observed in the present work, although part of the Na-cellulose seems also to be reversible. The spread of the published 004 peak positions suggests therefore that they cannot be used for deducing different Na-cellulose phases from the present data. It should also be noted that a reduction of Na-content in Na-cellulose due to washing with HCl droplets (see below) results in a systematic change of the peak position towards the cellulose I peak. This shows that the 004 peak position is indeed sensitive to the Na-content, which might be of interest in the context of future in-situ studies.

In Fig.25 the variation of integrated intensities and fwhm-values in radial direction of the equatorial 200 reflections of cellulose I and Na-cellulose across the transition zone are shown.[18]

[18] Scan 6; Annex C; mesh-width: 15_h*3.5_v µm^2; note that the intensities were summed in vertical direction as described previously in order to obtain a better counting statistics.

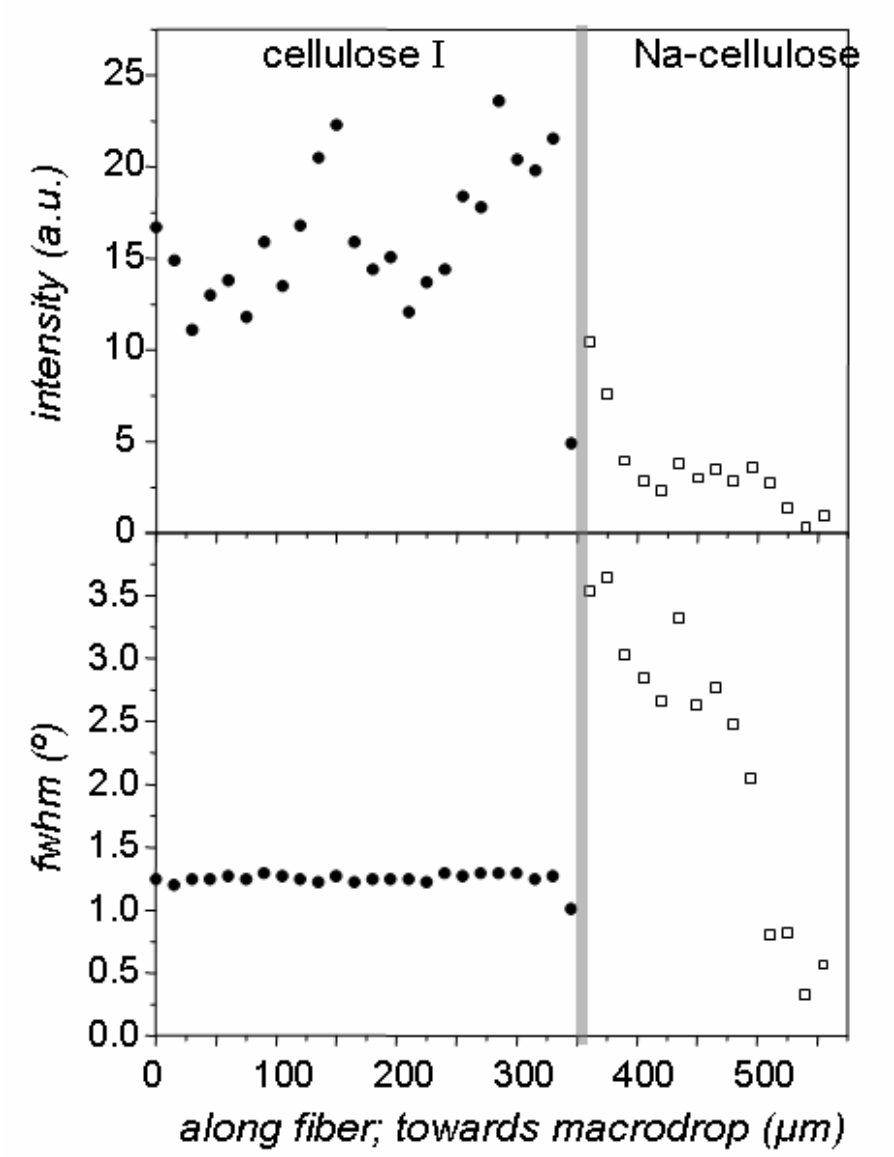

Fig.25 Evolution of integrated intensities and fwhm-values across the transformation zone from cellulose I to Na-cellulose for Scan 6.

The variation of integrated intensities shows a sharp phase limit for a step-width of 15 µm along the fiber. Interestingly, the fwhm values of the Na-cellulose peak are significantly higher than those of cellulose I at the phase limit but drop below the cellulose I value towards the macrodrop. As the peak width is roughly inversely proportional to the particle size (Scherrer formula: [68]) one has to assume that the Na-cellulose particle size is at the phase limit smaller than that of cellulose I and increases above the cellulose I value towards the macrodrop. This seems to directly support the mechanism of formation of Na-cellulose domains by a nucleation/growth process in the amorphous parts between the nanocrystalline domains [33], where crystallites form in sizes depending on the provided amount of NaOH.

An alternative approach of reducing the alkaline content in the fiber is by 0.5N HCl droplets. The experiment was performed by initially exposing a single cotton fiber to a NaOH macrodrop for about 30 min. and subsequently replacing the aqueous microdrops for about 30 min. against 0.5N HCl microdrops. The parameters of the mesh-scan were 15_h*3.5_v µm^2.[19] NaCl precipitation was observed for the whole range of Na-cellulose formation. A single pattern from the vicinity of the macrodrop shows both Na-cellulose and NaCl peaks (Fig.26.A). It is interesting to note that the NaCl precipitation shows a high texture (Fig.26.B, top), which suggests that this is due to NaCl crystallizing epitaxially on the cellulose microfibrils. A more detailed analysis of the phases formed has not been attempted in the context of the present work.

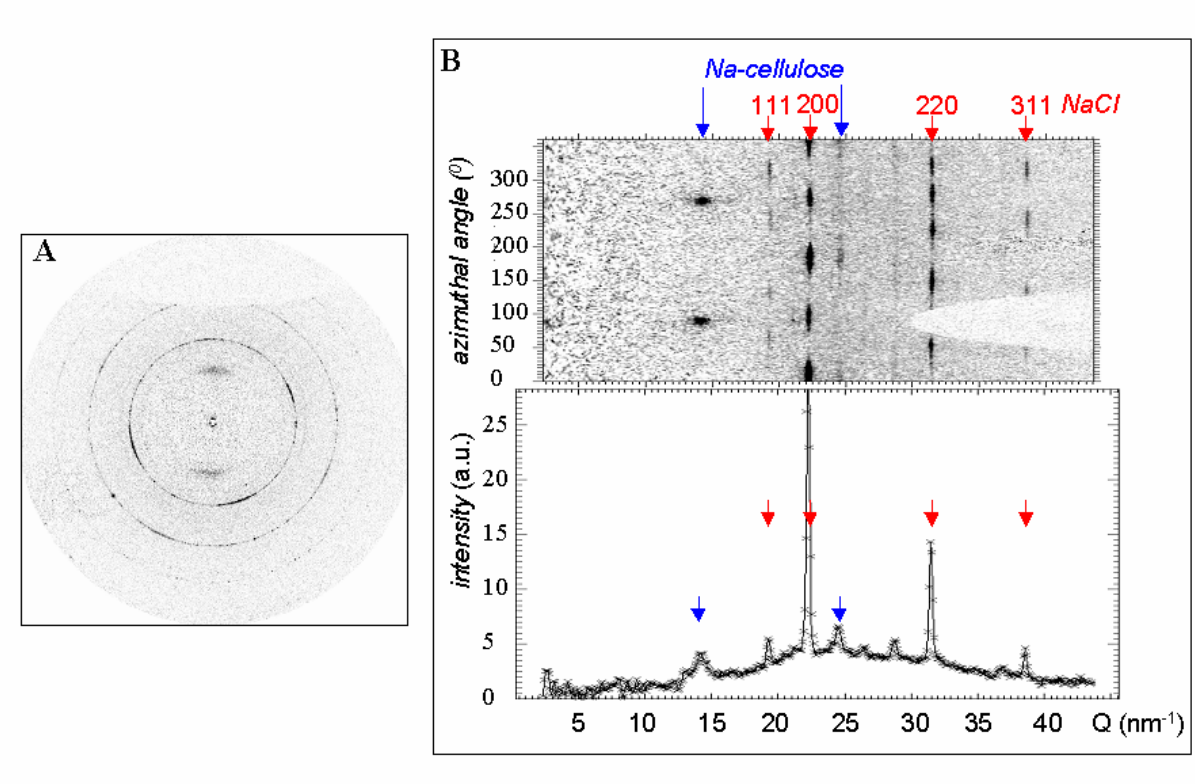

Fig.26 A: pattern of Na-cellulose, which has been exposed to 0.5N HCl microdrops; B-top: azimuthally regrouped pattern; B-bottom: azimuthally averaged pattern; the strongest NaCl and Na-cellulose peaks have been marked.

Fig.27 depicts schematically the current understanding of the transformation of the cotton fiber for the reaction conditions used in the present work. It is assumed that the NaOH concentration in the macrodrop has reached saturation and that the solid NaOH*H_2O crust on its surface limits further evaporation. One can also assume

[19] Scan 7; Annex C

that NaOH solution will diffuse into the solid fiber as observed for H_2O diffusion into the fiber (see above). The diffusion of aqueous NaOH into the fiber is accompanied by reaction to Na-cellulose. The simplest explanation for the observation of a spatial limitation of the Na-cellulose formation is for a reduction in NaOH concentration along the fiber or due to an evaporation of the solvent (H_2O) from the fiber to the air. This would result in a concentration and precipitation of NaOH along the diffusion direction, which is also observed experimentally.

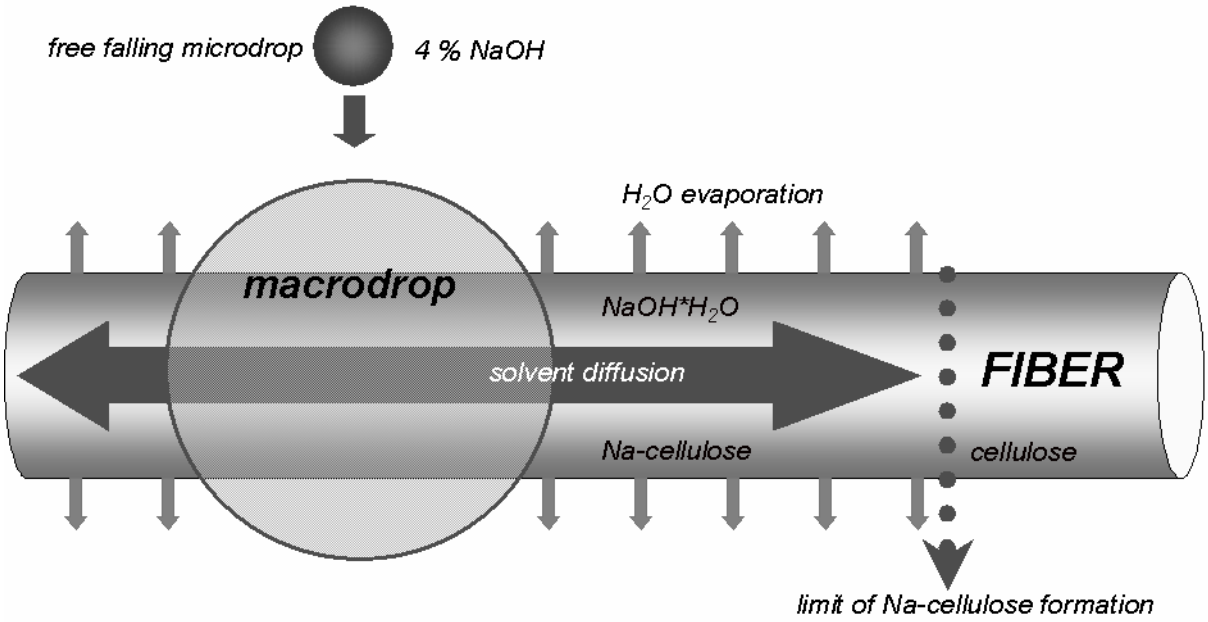

Fig.27 Schematic design of cotton fiber transformation.

5.4 Formation of other alkali-cellulose phases

An extensive literature on the swelling of cotton fibers by alkaline agents exists [10]. Structural data are, however, not existing or not easily accessible. It was therefore decided to study the extent of structural transformation of a cotton fiber for selected alkaline, and one earth-alkaline, agents shown in Fig.28.A. The treatments with the alkali-solutions and their concentrations are listed in Annex A.

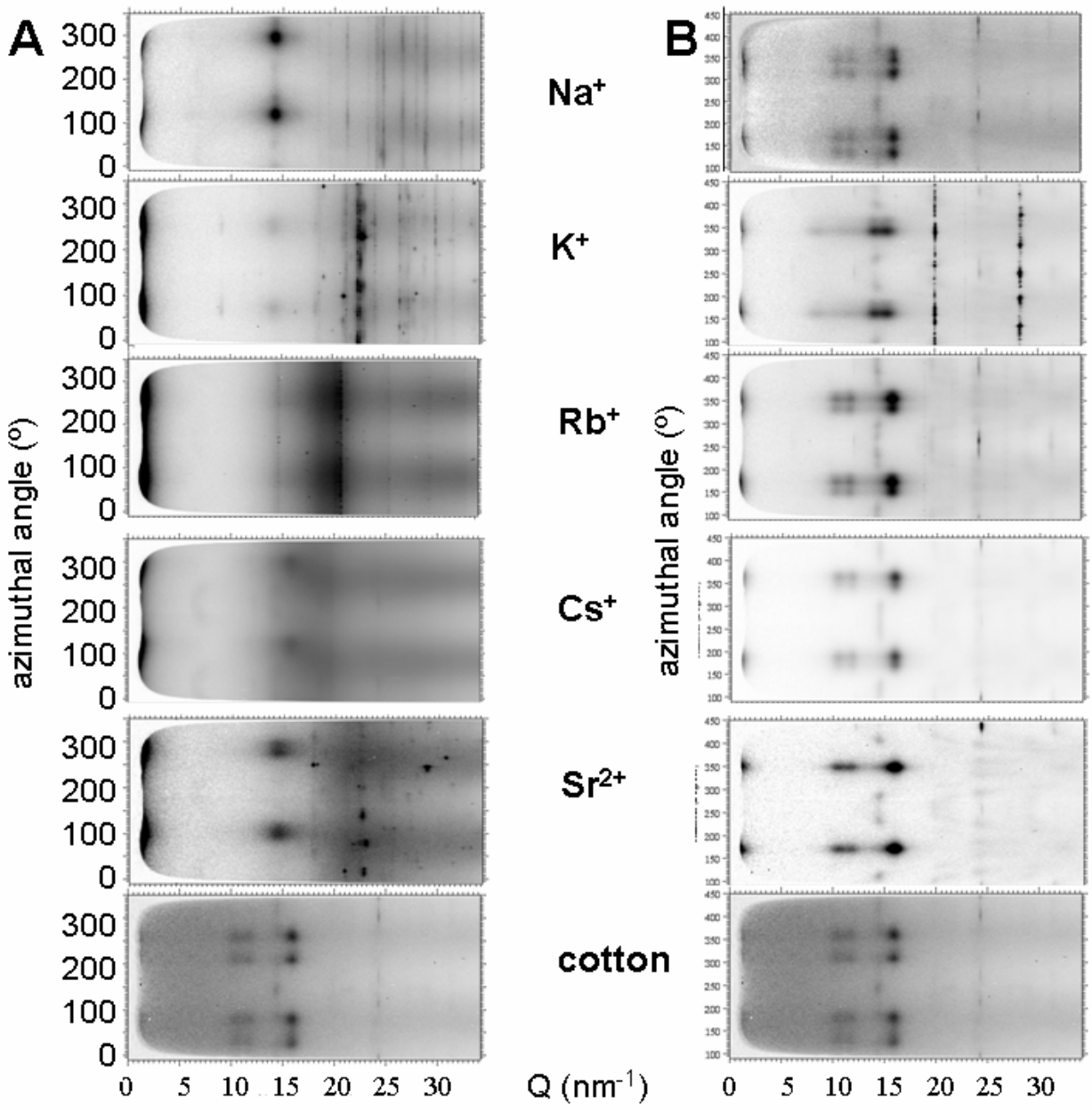

Fig.28 Images of a range of different alkaline and earth alkaline intercalates of cotton A: intercalate; B: after washing with 1 N HCl.

It is interesting to note that the fiber structure is modified in all cases but that the original cellulose I structure is always recuperated after washing with 1N HCl (Fig.28.B). The crystallinity differs, however, for the different phase as evidenced by the strongest equatorial peaks or the diffuse background and seems to be highest for Na^+ and Sr^{2+} swelling.

6 Conclusion and outlook

In this Master thesis the use of a microdrop generator for initiating the reaction of single cotton fibers with water and alkaline solutions has been investigated. The use of microdrops has allowed starting diffusional and transformational processes on a highly local scale, which could be probed by synchrotron radiation microdiffraction. The use of a stretching cell as sample support allowed an easy positioning of the fiber in the beam and maintaining the position during a stress-controlled experiment. Furthermore, changes in length due to the transformation could be easily monitored.

The major results of the present study are:

Upon washing of Na-cellulose much of it is retransformed to Cellulose I under the presented conditions, moving the phase boundary closer to the macrodrop. According to literature this can be explained by two different Na-cellulose I structures, one of which can return to the Cellulose I structure, while the other one can not. However, this is not incontestably proven by the analyzed data.

Cellulose II was not observed, probably due to the closed nature of the system and retention of NaOH concentration in it, where only H_2O evaporates.

It was shown that the 004 peak position of Na-cellulose is indeed sensitive to the Na-content as can be deduced from its variation on washing with HCl.

The analysis of the FWHM suggests that the Na-cellulose crystallite size is bigger than cellulose I crystallite size inside of and close to the NaOH macrodrop, but decreases rapidly with increased distance, down to sizes smaller than cellulose I crystallites. This supports the domain-growth process in the amorphous regions suggested in literature.

Other alkaline bases were found to also retransform in a great part to the Cellulose I structure, albeit with differing crystallinity.

The experiments have been limited until now to ex-situ studies of cotton fibers after aqueous alkali treatment and after H_2O-washing or HCl-neutralization by microdrops. Kinetic experiments could be performed - as shown for starch hydration [7] - by monitoring the formation of Na-cellulose at a given distance from the center of a macrodrop. The sub-μm beam size used for the scanning experiments would have allowed a higher spatial resolution study of the cellulose I/Na-cellulose transition

zone. Such studies will, however, have to be performed at low temperatures [7] in order to limit radiation damage effects.

Annex A: Preparation of solutions and fibers

Preparation of NaOH solution:

All NaOH solutions were prepared using dry NaOH pellets, which were weighted and dissolved in distilled water. The solutions were stored in airproof bottles and out of sunlight.

Preparation fibers for mounting on glass capillary:

- Fiber A: 4h in 10 mass-% NaOH, 6h in 1N HCl, washed in H_2O, air-dried
- Fiber B: 6h in 10 mass-% NaOH, 60h in 1N HCl, washed in H_2O, air-dried
- Fiber C: 16h in 0.06N $Sr(OH)_2$, 20h in 1N HCl, washed in H_2O, air-dried
- Fiber D: 16h in 8N KOH, 20h in 1N HCl, washed in H_2O, air-dried
- Fiber E: 1h in 10% NaOH, 15min in 1N HCl, washed in H_2O, air-dried
- Fiber F: 52h in 20% NaOH
- Fiber G: 2h in 8N KOH
- Fiber H: 2h in 0.05N $Sr(OH)_2$
- Fiber K: 15min in 0.78 RbOH, 15min in 1N HCl, washed in H_2O, air-dried
- Fiber L: 15min in 0.67N CsOH, 15min in 1N HCl, washed in H_2O, air-dried

Annex B: Practical aspects of microdrop generator

General information on microdrop generation can be found in ref. [56].

The microdrop generator used in the present study consists of a head and a control unit from Microdrop, Norderstedt, Germany. Different heads were used with similar properties (droplet sizes for all models ~50µm). Some heads had a heating coil incorporated, but the viscosities of H_2O, NaOH and HCl were low enough to be used at room temperature. Experiments were performed in experimental hutch II using the scanning set-up. A TTL signal-controlled by the beamline control SPEC software- was used to trigger microdrop generation with bursts of one to four droplets per pulse. The resulting macrodrop on the fiber was monitored with an optical microscope and the desired position for the scan selected. Different settings for the pulse force and duration were possible with the control unit, but for this work only the creation of a macrodrop on the fiber mattered.

Cleaning of the heads was necessary from time to time to avoid clogging and a splitting of the droplets at ejection. This was done by washing the head and tube from the muzzle to the tank with demineralized H_2O and concentrated NaOH and HCl. In the ID13 laboratory, tests were monitored with a stroboscopic diode, which allowed “freezing” of the image for recording with a microscope camera. The shape of the droplets and the beam of droplets were checked to assure that the droplets were intact and ejected straight from the nozzle.

Annex C: Files and Dates

Number	Date	File name	scan type	[µm] dimension	medium
Scan 1	04.3.06	cotton_waterdropon_scan12…	mesh	0.2 x 0.03	H_2O
Scan 2	20.3.06	cotton_20306_90mmdet_10…	mesh	0.75 x 0.08	NaOH
Scan 3	20.3.06	cotton_20306_90mmdet_11…	mesh	0.75 x 0.08	NaOH & H_2O
Scan 4	20.3.06	cotton_20306_90mmdet_13…	mesh	0.75 x 0.084	NaOH
Scan 5	20.3.06	cotton_20306_90mmdet_14…	mesh	0.75 x 0.126	NaOH & H_2O
Scan 6	29.4.06	drop_fiber2_29406_3…	mesh	0.75 x 0.084	NaOH
Scan 7	29.4.06	drop_fiber3_29406_1…	mesh	0.6 x 0.084	NaOH & HCl
Scan 8	30.4.06	drop_fiber4_300406_1…	mesh	0.6 x 0.084	NaOH

Literature

1. Okano, T. and A. Sarko, *Mercerization of cellulose 1. X-ray diffraction evidence for intermediate structures.* J. Appl. Polym. Sci., 1984. **29**: p. 4175-4182.
2. Okano, T. and A. Sarko, *Mercerization of cellulose. 2. Alkali-cellulose intermediates and a possible mercerization mechanism.* J. Appl. Polym. Sci., 1985. **30**: p. 325-332.
3. Nishimura, H., T. Okano, and A. Sarko, *Mercerization of Cellulose. 5. Crystal and Molecular Structure of Na-Cellulose I.* Macromolecules, 1991. **24**: p. 759-770.
4. Riekel, C., *New Avenues in X-ray microbeam experiments.* Rep. Prog. Phys., 2000. **63**: p. 233-262.
5. Riekel, C., et al., *Combined microdrop generation and microdiffraction for biopolymer hydration experiments.* Fibre Diffraction Review, 2004. **12**: p. 36-40.
6. Rössle, M., et al., *Fast intra-crystalline hydration of β-chitin revealed by a combined microdrop generation and on-line synchrotron radiation microdiffraction.* Biomacromolecules, 2003. **4**: p. 981-986.
7. Lemke, H., et al., *Structural Processes during Starch Granule Hydration by Synchrotron Radiation Microdiffraction.* Biomacromolecules, 2004. **5**(4): p. 1316-1324.
8. CERMAV-CNRS. *http://www.cermav.cnrs.fr/glyco3d/*, 2005. Retrieved 06. - 07.2006.
9. Klemm, D., et al., *Comprehensive Cellulose Chemistry*. Vol. 1. 1998, Weinheim (BRD): Wiley-VCH.
10. Warwicker, J.O., et al., *A Review on the Literature on the Effect of Caustic Soda and Other Swelling Agents on the Fine Structure of Cotton*, ed. T.C.S.A.M.-M.F.R. Association. 1966, Manchester: Shirley Institute.
11. Chu, S.S.C. and G.A. Jeffrey, *The refinement of the crystal structures of β-D-glucose and cellobiose.* Acta Cryst., 1968. **24**: p. 830-838.
12. Atalla, R.H. and D.L. VanderHart, *Native cellulose : a composite of two distinct crystalline forms.* Science, 1983. **223**: p. 283-285.
13. Finkenstadt, V.L. and R.P. Millane, *Crystal structure of Valonia cellulose Ib.* Macromolecules, 1998. **31**: p. 7776-7783.
14. Nishiyama, Y., P. Langan, and H. Chanzy, *Crystal structure and hydrogen bonding system in cellulose 1β from synchrotron X-ray and neutron fiber diffraction.* J. Am. Chem. Soc., 2002. **124**: p. 9074-9082.
15. Nishiyama, Y., et al., *Crystal structure and hydrogen bonding system in cellulose 1α, from synchrotron X-ray and neutron fiber diffraction.* J. Am. Chem. Soc., 2003. **125**: p. 14300-14306.
16. Gardner and J. Blackwell, *The structure of native cellulose.* Biopolymers, 1974. **13**: p. 1975-2001.
17. Hess, K. and C. Trogus, Chem. Ber., 1935. **68**: p. 1986-1988.
18. Kulshreshtha, A.K., J. Text. Inst., 1979. **1**: p. 13-18.
19. Wada, M., et al., *Cellulose III_I Crystal Structure and Hydrogen Bonding by Synchrotron X-ray and Neutron Fiber Diffraction.* Macromolecules, 2004. **37**: p. 8548-8555.

20. Wada, M., L. Heux, and J. Sugiyama, *Polymorphism of Cellulose I Family: Reinvestigation of Cellulose IVI.* Biomacromolecules, 2004. **5**: p. 1385-1391.
21. Gardiner, E.S. and A. Sarko, *Packing analysis of carbohydrates and polysaccharides. 16. The crystal structures of cellulose IVI and IVn.* Can. J. Chemistry, 1985. **63**: p. 173-180.
22. Klemm, D., H.P. Schmauder, and T. Heinze, *Cellulose*, in *Polysaccharides*, A. Steinbüchel, S.D. Baets, and E. Vandamme, Editors. 2002, Wiley-VCH Verlag GmbH: Weinheim. p. 275-319.
23. Butterfield, B.G., ed. *Microfibril Angle in Wood*. 1997, University of Canterbury: Christchurch, New Zealand.
24. Lichtenegger, H., et al., *Imaging of the helical arrangement of cellulose fibrils in wood by synchrotron radiation X-ray microdiffraction.* J. Appl. Cryst., 1999. **32**: p. 1127-1133.
25. Sugiyama, J., R. Vuong, and H. Chanzy, *Electron diffraction study on the crystalline phases occuring in native cellulose from algal cell wall.* Macromolecules, 1991. **24**: p. 4168-4175.
26. Sarko, A. and R. Muggli, *Packing analysis of carbohydrates and polysaccharides. 3. Valonia cellulose and cellulose II.* Macromolecules, 1974. **7**: p. 486-494.
27. Chanzy, H. and B. Henrissat, *Unidirectional degradation of Valonia cellulose microcrystals subjected to cellulase action.* FEBS Lett., 1985. **184**: p. 285-288.
28. Raymond, S., A. Kvick, and H. Chanzy, *The structure of cellulose II: a revisit.* Macromolecules, 1995. **28**: p. 8422-8425.
29. Stipanovic, A.J. and A. Sarko, *Packing analysis of carbohydrates and polysaccharides. 6. Molecular and crystal structure of regenerated cellulose II.* Macromolecules, 1976. **9**: p. 851-857.
30. Kolpak, F.J. and J. Blackwell, *Determination of the structure of cellulose II.* Macromolecules, 1976. **9**: p. 273-278.
31. Gessler, K., et al., *β-D cellotetraose hemihydrate as a structural model for cellulose II. An X-ray diffraction study.* J. Am. Chem. Soc., 1995. **117**: p. 11397-11406.
32. Langan, P., Y. Nishiyama, and H. Chanzy, *A revised structure and hydrogen-bonding system in cellulose II from a neutron fiber diffraction analysis.* J. Am. Chem. Soc., 1999. **121**: p. 9940-9946.
33. Nishiyama, Y., S. Kuga, and T. Okano, *Mechanism of mercerization revealed by X-ray diffraction.* J. Wood Science, 2000. **46**: p. 452-457.
34. Nishimura, H. and A. Sarko, *Mercerization of cellulose. 3. Changes in crystallite sizes.* J. Appl. Polym. Sci., 1987. **33**: p. 855-866.
35. Revol, J.F., A. Dietrich, and D.A.I. Goring, *Effect of mercerization on the crystallite size and crystallinity index in cellulose from different sources.* Can. J. Chem., 1987. **65**: p. 1724-1725.
36. Crawshaw, J., et al., *Simultaneous SAXS and WAXS Investigations of Changes in Native Cellulose Fiber Microstructure on Swelling in Aqueous Sodium Hydroxide.* J. Appl. Pol. Sci., 2002. **89**: p. 1209-1218.
37. Dinand, E., et al., *Mercerization of primary wall cellulose and its implication for the conversion of cellulose I to cellulose II.* Cellulose, 2002. **9**: p. 7-18.
38. Beaudet, Tom, *What is Mercerized Cotton?*. FiberArts.org, 1999. Retrieved on 27.3.2007.
39. Kim, N.H., J. Sugiyama, and T. Okano, *X-ray and Electron Diffraction Study of Na-cellulose I: Formation and its reconversion back to cellulose I.* Mokuzai Gakkaishi, 1990. **36**(2): p. 120-125.

40. Baruchel, J., et al., eds. *Neutron and Synchrotron Radiation for Condensed Matter Studies*. Neutron and Synchrotron Radiation for Condensed Matter Studies. Vol. 1. 1993, Springer Verlag: Berlin. 79-94.
41. Lindner, P. and T. Zemb, eds. *Neutrons, X-Rays and Light: Scattering Methods Applied to Soft Condensed Matter*. 2002, North-Holland: Amsterdam.
42. Catlow, C.R.A. and G.N. Greaves, eds. *Applications of Synchrotron Radiation*. 1990, Blackie: Glasgow.
43. Nave, C. and E.F. Garman, *Towards an understanding of radiation damage in cryocooled macromolecular crystals.* J. Synchotron Rad., 2005. **12**: p. 257-260.
44. Nave, C. and M.A. Hill, *Will reduced radiation damage occur with very small crystals?* J. Synchotron Rad., 2005. **12**: p. 299-303.
45. Sawyer, L.C., et al., *Microfibrillar structures in liquid-crystalline polymers.* J. Mat. Sci., 1993. **28**: p. 225-238.
46. Sawyer, L.C. and D.T. Grubb, *Polymer Microscopy*. 1996, London: Chapman&Hall.
47. Giacovazzo, G., ed. *Fundamentals of Crystallography*. 1992, Oxford University Press: New York.
48. Müller, M., et al., *Direct observation of Microfibril Arrangement in Single Native Cellulose Fiber by Microbeam Small-Angle X-Ray Scattering.* Macromolecules, 1998. **31**: p. 3953-3957.
49. Stein, R.S. and G.L. Wilkes, *Physico-Chemical Approaches to the Measurement of Anisotropy*, in *Structure and Properties of Oriented Polymers*, I.M. Ward, Editor. 1975, Applied Science Published Ltd: London. p. 57-145.
50. Müller, M., et al., *Skin/core micro-structure in viscose rayon fibres analysed by X-ray microbeam and electron diffraction mapping.* Polymer, 2000. **41**(7): p. 2627-2632.
51. Perrakis, A., et al., *Protein microcrystals and the design of a diffractometer: current experience and plans at EMBL and ESRF/ID13.* Acta Cryst., 1999. **D55**: p. 1765-1770.
52. Schroer, C.G., et al. *Beryllium parabolic refractive X-ray lenses*. 2002: SPIE.
53. David, C., B. Noehammer, and E. Ziegler, *Wet etching of linear Fresnel zone plates for hard X-rays.* Microelectronic Engineering, 2002. **61-62**(i): p. 987-992.
54. deGruy, I.V., J.H. Carra, and W.R. Goynes, *The Fine Structure of Cotton; an Atlas of Cotton Microscopy*, in *Fiber Science Series*, R.T. O'Connor, Editor. 1973, Marcel Dekker: New York.
55. Davies, R.J., et al., *Single fibre deformation studies of poly(p-phenylene benzobisoxazole) fibres.* J. of Mater. Sci., 2001. **36**: p. 3079-3087.
56. Lee, E.R., *Microdrop Generation*. Nano- and Microscience, Engineering, Technology, and Medicine Series, ed. S.E. Lyshevski. 2003, Boca Raton: CRC Press.
57. Hammersley, A., *FIT2D-V10.3*, in *http://www.esrf.fr/computing/scientific/FIT2D/*.
58. Gourrier, A., *Etudes Combinees de microdeformation par indentation et de microdiffraction des rayons-X: applications dans le cas de polymeres.*, in *Physics*. 2004, Universite Joseph Fourier: Grenoble.
59. Davies, R., *A new batch-processing data-reduction application for X-ray diffraction data.* J. Appl. Cryst., 2006. **39**: p. 267-272.
60. Wada, M., T. Okano, and J. Sugiyama, *Synchrotron-radiated X-ray and neutron diffraction study of native cellulose.* Cellulose, 1997. **4**: p. 221-232.

61. Meyer, K.H. and L. Misch, *Position des atomes dans le nouveau module spatial de la cellulose.* Helv. Chim. Acta, 1937. **20**: p. 232-244.
62. Sobue, H., H. Kiessig, and K. Hess, *Das System-Natriumhydroxyd-Wasser in Abhaengigkeit von der Temperatur.* Z. Phys. Chemie, Abt. B, 1939. **43**(5): p. 309-328.
63. Linke, W.F., *Solubilities, inorganic and metal organic compounds*. Vol. II. 1965, Washington: Am. Chem. Soc.
64. Kim, N.H., J. Sugiyama, and T. Okano, *X-ray and Electron Diffraction Study of Na-cellulose I; The effect of wahing temperature on the structure of Na-cellulose I.* Mokuzai Gakkaishi, 1991. **37**(7): p. 637-643.
65. Rustad, J.R., et al., *Ab initio investigation of the structures of NaOH hydrates and their Na+ and OH- coordination polyhedra.* American Mineralogist, 2003. **88**: p. 436-449.
66. Jacobs, H. and U. Metzner, *Ungewoehnliche H-Brueckenbindung in Natriumhydroxidmonohydrat: Roentgen und Neutronenbeugung an NaOH*H2O bzw. NaOD*D2O.* Zeitschrift f. Anorganische und Allgemeine Chemie, 1991. **597**: p. 97-106.
67. Hayashi, J., T. Yamada, and K. Kimura, *The change of the chain conformation of cellulose from type I to II.* J. Appl. Pol. Sci. Sympo., 1976. **28**: p. 713-727.
68. Klug, H.P. and L.E. Alexander, *X-ray diffraction procedures for polycrystalline and amorphous materials*. 2nd ed. 1974, New York, N.Y.: Wiley Interscience.

Acknowledgements

I would like to thank several people who made it possible for me to conduct my master thesis project at the ESRF and were a great help with every problem that got in the way.

- Prof. Dr. Hans-Peter Steinrück, FAU Erlangen-Nürnberg, for communicating the traineeship and being my tutor
- Dr. Christian Riekel for providing me the position and for all his help, advice and collaboration during the whole project
- Dr. Richard Davies for his data analysis software and many answered questions
- Dr. Manfred Burghammer for great beamline maintenance
- Anne Martel for introducing me into the area and collaboration with some experiments
- Lionel Lardiere for technical assistance and handiwork
- Everyone at ID13 for a good time

Declaration

Hereby I confirm that I conducted this work myself, using the cited sources and aids. This project has been realized in collaboration with members of the ESRF ID13 group.

(Johannes Manuel Schöck)